Aerosol activation characteristics and prediction at the central European ACTRIS research station Melpitz, Germany

Yuan Wang[1,2,3*], Silvia Henning[1*], Laurent Poulain[1], Chunsong Lu[2], Frank Stratmann[1], Yuying Wang[2], Shengjie Niu[2,4], Mira L. Pöhlker[1], Hartmut Herrmann[1], and Alfred Wiedensohler[1]

1. Leibniz Institute for Tropospheric Research (TROPOS), 04318 Leipzig, Germany.
2. Collaborative Innovation Center on Forecast and Evaluation of Meteorological Disasters, Nanjing University of Information Science and Technology, 210044 Nanjing, China.
3. Collaborative Innovation Center for Western Ecological Safety, Lanzhou University, 730000 Lanzhou, China.
4. College of Safety Science and Engineering, Nanjing Tech University, 210009 Nanjing, China.

*Correspondence: Yuan Wang (wang_yuan@lzu.edu.cn) and Silvia Henning (henning@tropos.de)

Abstract: Understanding aerosol particle activation is essential for evaluating aerosol indirect effects (AIEs) on climate. Long-term measurements ~~on~~ of aerosol particle activation help to understand the AIEs and narrow down the uncertainties of AIEs simulation~~;~~. H~~h~~owever, they are still scarce. In this study, more than 4-year aerosol comprehensive measurements were utilized at the central European research station Melpitz, Germany, to gain insight into the aerosol particle activation and provide recommendations on improving the prediction of number concentration of cloud condensation nuclei (CCN, N_{CCN}). As supersaturation (SS) increases from 0.1% to 0.7%, the median N_{CCN} increases from 399 to 2144 cm^{-3}, which represents 10% to 48% of the total particle number concentration with a diameter range of 10 – 800 nm, while the median hygroscopicity factor (κ) and critical diameter (D_c) decrease from 0.27 to 0.19 and from 176 to 54 nm, respectively. Aerosol particle activation is highly variable across seasons, especially at low SS conditions. At SS = 0.1%, the median N_{CCN} and

activation ratio (AR) in winter are 1.6 and 2.3 times higher than the summer values, respectively. Both κ and the mixing state are size dependent. As the particle diameter (D_p) increases, κ increases at D_p of ~40 to 100 nm and almost stays constant at D_p of 100 to 200 nm, whereas the degree of the external mixture keeps decreasing at D_p of ~40 to 200 nm. The relationships of κ vs. D_p and degree of mixing vs. D_p were both fitted well by a power-law function. Size-resolved κ improves the N_{CCN} prediction. We recommend applying the κ - D_p power-law fit for N_{CCN} prediction at Melpitz, which performs better than using the constant κ of 0.3 and the κ derived from particle chemical compositions and much better than using the N_{CCN} (AR) vs. *SS* relationships. The κ - D_p power-law fit measured at Melpitz could be applied to predict N_{CCN} for other rural regions. For the purpose of improving the prediction of N_{CCN}, long-term monodisperse CCN measurements are still needed to obtain the κ - D_p relationships for different regions and their seasonal variations.~~The overall characteristics of aerosol particle activation at Melpitz are first summarized. For supersaturation (*SS*) levels of 0.1%, 0.2%, 0.3%, 0.5%, and 0.7%, the mean cloud condensation nuclei (CCN) number concentration (N_{CCN}) increases with the increase of *SS* from 513 to 2477 cm^{-3}, which represents 11% to 52% of the total particle number concentration with diameter ranging from 10 to 800 nm, while the hygroscopicity factor (κ) and the critical diameter (D_c) decrease from 0.28±0.08 (mean value ± one standard deviation) to 0.20±0.09 and from 177±19 to 54±8 nm, respectively. Aerosol particle activation is highly variable across seasons, especially at low *SS* conditions. At *SS* = 0.1%, the seasonal mean N_{CCN} is 681 cm^{-3} in winter, which is almost twice higher than the summer value (347 cm^{-3}); the seasonal mean activation ratio (AR) in winter (0.18) is three times higher than the summer one. Subsequently, size dependency of both κ and the state of mixing were~~

~~investigated. As the particle diameter (D_p) increases, κ increases at D_p of ~40 to 100 nm and almost stays constant at D_p of 100 to 200 nm, whereas the degree of the external mixture keeps decreasing at D_p of ~40 to 200 nm. The relationships of κ vs. D_p and mixture degree vs. D_p were both fitted well by the power-law function for each season. Finally, we recommend applying the κ - D_p power-law fit for N_{CCN} prediction, which can narrow down the median uncertainty within 10% for different *SS* conditions and seasons at Melpitz; it also could be applied to predict N_{CCN} at other rural and continental regions with a similar aerosol background. Additionally, the mean κ value over D_p of 100 to 200 nm also works well on the N_{CCN} prediction when *SS* is less than 0.2%.~~

1. Introduction

The specific subset of aerosol particles that serves as nuclei for the condensation of water vapor, forming cloud droplets at a given supersaturation (*SS*) condition, is known as cloud condensation nuclei (CCN). Aerosol particle activation affects the aerosol and cloud interactions (ACI), thereby changing the cloud microstructure (Zhao et al., 2012; Jia et al., 2019; Wang et al., 2019), precipitation (Khain, 2009; Wang et al., 2011; Fan et al., 2012, 2018), radiation (Twomey, 1974, 1977; Albrecht, 1989; Zhao and Garrett, 2015), and by these effects the global climate (Ramanathan et al., 2001; Rosenfeld et al., 2019). The latest sixth assessment report from IPCC (2021) pointed out that aerosol indirect effects (AIEs) remain the most considerable uncertainty in assessing the anthropogenic contribution to present and future climate change.

The ambient *SS* and aerosol activation ability are both important for predicting the number concentration of ~~activated~~ cloud droplets. The classical Köhler theory (Köhler, 1936), combining the Raoult law with the Kelvin effect, illustrates that the aerosol particle activation depends on particle size, chemical composition and the given *SS*. Petters and Kreidenweis (2007) parameterized the Raoult term with a single

hygroscopicity factor κ to capture the water activity without needing to know anything about the dissolved compounds.~~Petters and Kreidenweis (2007) utilized a single hygroscopicity factor κ to describe the CCN activity at each particle diameter (D_p), which facilitates studying the activation process without considering the complex chemical compositions of aerosol particles (McFiggans et al., 2006)~~. ~~–~~Different perspectives have been presented on the influence of particle size and composition on the CCN activation. In terms of a single aerosol particle, the actual particle size plays a more important role than the chemical composition for activation because of the different range in which κ and particle diameter (D_p) vary and the reciprocal relationship between κ and the third power of the critical D_p (D_c^3)~~D_p^3~~ at a given SS. As for a population of aerosol particles, Dusek et al. (2006) concluded that particle number size distribution (PNSD) matters more than the chemical composition distribution, which has been supported by many experiments. Even sometimes, assuming a constant κ still predicted CCN number concentration (N_{CCN}) well (e.g., Sihto et al., 2011; Wang et al., 2018a). Andreae and Rosenfeld (2008) reviewed the previous studies on aerosol particle activation and recommended that for modeling purposes, the global κ values of 0.3±0.1 and 0.7±0.2 can be representative for continental and marine aerosol, respectively, which has been widely used to predict N_{CCN}. The regional variability should be ~~underlined~~ emphasized because the mean κ measured in urban, rural, and forest exhibits significant differences. For instance, Sihto et al. (2011) suggested an average κ of 0.18 to predict the CCN activation well in boreal forest conditions in Hyytiälä, Finland~~;~~. ~~a~~ A fixed κ of 0.31 suffices to calculate the N_{CCN} in a suburban site located in the center of the North China Plain (Wang et al., 2018a~~);~~). ~~the~~ The mean κ is 0.5 in a near-coast background station (CESAR Tower) in Netherlands (Schmale et al., 2018).~~;~~ ~~the~~ The median κ ranges from 0.02 to 0.16 at SS = 0.1−1.0% in an urban background site in

Budapest, Hungary (Salma et al., 2021). Therefore, the assumption of a constant κ = 0.3 may not be appropriate when trying to predict N_{CCN} for different continental regions.

Additionally, some experiments, especially conducted on more diverse particulate sources, have indicated chemistry does play an important role in N_{CCN} variability (e.g., Nenes et al., 2002; Petters and Kreidenweis, 2007; Rose et al., 2010). Not only the bulk chemical composition with a constant κ should be considered for N_{CCN} prediction, but the size-resolved chemical composition (Deng et al., 2011; Wu et al., 2016) and the mixing state should be applied (Su et al., 2010; Zhang et al., 2014). Information on the organic aerosol fraction improves N_{CCN} prediction considerably (Poulain et al., 2010; Zhang et al., 2016; Kuang et al., 2020). Freshly formed particles are about 1 nm in diameter (Kulmala et al., 2012)~~; they~~, which must grow to tens of nanometers in diameter to serve as the effective CCN at a relatively high *SS* of ~1% (Dusek et al., 2006) and even larger than 200 nm to be efficient at *SS* less than 0.1% (Deng et al., 2013). Aerosol chemical composition changes during the growing and aging processes. For instance, κ increases with particle size caused by photochemical processes which enhancing secondary inorganic species formation and going along with an increase in particle size (Massling et al., 2009; Zhang et al., 2017; Wang et al., 2018b). On the other hand, in sulfate dominated new particle formation (NPF) events with subsequent particle growth by condensation of organic vapors, the κ of small particles may exceed the κ of the larger ones (Wang et al., 2018a). If the κ of organic aerosol increases from 0.05 to 0.15, the global average aerosol radiative forcing would decrease by ~1 W m^{-2}, which is in the same order of magnitude as the overall climate forcing of anthropogenic aerosol during the industrialization period (Rastak et al., 2017).

To obtain the regional parameters of aerosol particle activation, extensive field campaigns have been conducted worldwide. Besides the significant difference in spatial,

also the temporal variations of aerosol activation characteristics are essential for N_{CCN} prediction (Andreae and Rosenfeld, 2008). Most of the observations lasted 1–2 months or even less~~;~~ , ~~they~~ mainly ~~focused~~ focusing on the effects of short-term weather processes or pollution events on aerosol particle activation, such as the effects of the summer monsoon (Jayachandran et al., 2020), wet removal (Croft et al., 2009), NPF events (Dusek et al., 2010; Wu et al., 2015), biomass burning (Rose et al., 2010), and aerosol particle aging as well as oxidation processes (Zhang et al., 2016, 2017). The long-term CCN measurements (of at least one full year) are still rarely reported, resulting in insufficient knowledge concerning the seasonal and annual cycles of aerosol particle activation, which are also critical for model predictions and evaluations. Burkart et al. (2011) reported the particle activation in the urban background aerosol of Vienna, Austria, based on 11-month aerosol and CCN concentration measurements. Paramonov et al. (2015) reported a synthesis of CCN measurements within the EUCAARI network using the long-term data collected at 14 locations. Pöhlker et al. (2016) presented the climatology of CCN properties of a remote central Amazonian rain forest site using 1-year measurements. Che et al. (2017) provided the aerosol-activation properties in the Yangtze River Delta, China, based on ~1-year measurements. Using the long-term (of most > 1 year) aerosol and CCN concentration measurements from 12 sites, Schmale et al. (2018) presented the spatial differences in aerosol particle activation for various regional backgrounds. However, systematic studies focusing on the seasonal cycle of size-resolved particle activation and respective CCN predictions are still scarce in the central European continent. Such a study would be of great help for understanding ACI and narrowing down the regional uncertainties in climate predictions.

In this investigation, more than 4-year comprehensive measurements of aerosol physical, chemical, and activation properties collected at the ACTRIS (Aerosol, Clouds and Trace Gases Research Infrastructure, http://www.actris.eu/) site Melpitz, Germany, are utilized. The major objective is to gain insight into the aerosol particle activation and provide recommendations on methods for N_{CCN} predictions. We present therefore the long-term observations and seasonal cycles of various particle activation variables such as ~~CCN number size distribution,~~ N_{CCN}, activation ratio, critical diameter, size-resolved κ and mixing state~~ degree~~. Furthermore, we evaluated the accuracy of N_{CCN} calculated from five different activation schemes and finally provide recommendations ~~to use a power-law based parameterization for the dependence of κ on particles diameter for long-term~~on N_{CCN} prediction at Melpitz and for other rural regions~~ with a similar aerosol background condition~~.

2. Methodology

2.1 Experiment details

Atmospheric aerosol measurements were conducted at the Melpitz observatory (51.54°N, 12.93°E, 86 m above sea level), 50 km to the northeast of Leipzig, Germany. The aerosol particles observed at Melpitz can be regarded as representative for the central European rural background conditions (Birmili et al., 2009). The surroundings of the site are mostly pastures and forests without significant sources of anthropogenic emissions. More detailed descriptions of the Melpitz site can be found~~ in~~, for example, in Poulain et al. (2020).

This study focuses on the physicochemical properties and the activation ability of aerosol particles using the data collected at Melpitz from August 2012 to October 2016. Figure 1 ~~demonstrates~~ shows the experimental setup. All instruments were in the same container laboratory and utilized the same air inlet. Ambient aerosol particles were first

pretreated through a PM_{10} Anderson inlet and an automatic aerosol diffusion dryer kept the relative humidity in sampling lines at a relative humidity less than 40%~~ (Tuch et al., 2009)~~ following the ACTRIS recommendations. Subsequently, the aerosol flow was divided into the different instruments using an isokinetic splitter. Particle number size distributions (PNSD) were measured using a Dual-mobility particle size spectrometer (D-MPSS, TROPOS-type; Birmili et al., 1999; Wiedensohler et al., 2012) with~~in the~~ a diameter ~~ranging~~ range ~~from~~ of 5 ~~–to~~ 800 nm. An aerosol chemical speciation~~species~~ monitor (ACSM, Aerodyne Inc; Ng et al., 2011) was used to measure the chemical compositions of the ~~near PM_1~~ non-refractory submicron aerosol particulate matter~~particles~~ (nitrate, sulfate, chloride, ammonium, and organics). A multi-angle absorption photometer (MAAP, model 5012, Thermo Scientific; Petzold and Schönlinner, 2004) was used to measure the particle light absorption coefficients and to estimate the equivalent black carbon (eBC) mass concentration. For simultaneous measurement of particle and CCN number size distributions, dried aerosol particles were passed through the bipolar charger to establish charge equilibrium (Wiedensohler, 1988) and then through a differential mobility analyzer (DMA) for selecting a monodisperse particle fraction~~; ~~. ~~after~~ After the DMA, the flow was ~~divided into two parts, respectively~~split to passed through a condensation particle counter (CPC, model 3010, TSI) to measure the total number concentration of the selected monodisperse condensation nuclei (N_{CN}) and through a cloud condensation nuclei counter (CCNC, model 100, Droplet Measurement Technologies; Roberts and Nenes, 2005) to measure the N_{CCN}. Thus, the size dependent activated fraction (AF, N_{CCN}/N_{CN}) curve, i.e., the AF at a certain diameter (D_p) of dry particles, could be obtained. The losses in both instruments were checked and it was corrected for in the inversion routine. The coupling between size selection and CCNC was programmed in a way that the size resolved

measurements started only after the temperature and thereby the *SS* of the CCNC was stabilized. As the diameter scan started after *SS* stabilization, the measurement itself was the same length at all *SS* conditions. At fully stabilized CCNC conditions we did one D_p scan at per *SS* setting. A total of five different *SS* conditions was set in the CCNC instrument (0.1%, 0.2%, 0.3%, 0.5%, and 0.7%). A complete *SS* cycle lasted ~2.5 hours~~.~~ and the slight variations in the 2.5h total *SS* cycle was only due to the waiting time until the temperature of the CCNC was stabilized.

All the instrumentation was frequently calibrated within the framework of the European Center for Aerosol Calibration (ECAC, https://www.actris-ecac.eu/). The ACSM was regularly calibrated according to the manufacturer's recommendations with 350 nm monodispersed ammonium nitrate and ammonium sulfate particles (Freney et al., 2019). The D-MPSS was calibrated following the recommendations in Wiedensohler et al. (2018). Throughout the campaign, the CCNC was~~ regularly~~ calibrated once a year following the procedures outlined in Rose et al. (2008) with using the E-AIM model (Clegg et al. 1998). The measurement uncertainties of these instruments should be noted. The uncertainty in the MAAP is within 10% (Müller et al., 2011), and those in the D-MPSS and CCNC are both on the order of 10% (Wiedensohler et al., 2018; Rose et al., 2008). For the *SS* setting in CCNC, Gysel and Stratmann (2013) pointed out that an achievable accuracy in *SS* is 10 % (relative) at *SS* > 0.2%, and less than 0.02 % (absolute) at the lower *SS*. For the ACSM data, the uncertainty in determining the total non-refractory mass is 9%.~~;~~ W~~w~~hile for the individual chemical components, the uncertainty~~it~~ is 15% for nitrate, 28% for sulfate, 36% for ammonium, and 19% for organic matter (Crenn et al., 2015).

Due to instrument failures and maintenance operations, missing measurements occurred during the campaign. Effective data coverage is shown in Figure S1 in

Supporting Information (SI)~~in Figure 2~~. Overall, the CCNC, D-MPSS, and ACSM-MAAP captured 45578 AF curves, 103052 PNSDs, and 26876-hour aerosol chemical measurements, which covered 63%, 92%, and 77% of the campaign time, respectively. For 42% of the time all these instruments were measuring together.

2.2 Methods

Each AF curve (N_{CCN}/N_{CN} vs. D_p) was first~~ly~~ corrected for multiply charged particles. Multiply (mostly doubly) charged particles appear in the AF curve as a plateau or shoulder at small diameters because they have the same electrical mobility diameter as singly charged smaller particles ~~; thus, they are falsely selected in the DMA~~ (Rose et al., 2008; Henning et al., 2014). To correct for this, the fraction of multiple charged particles as determined from the D-MPSS measurements was subtracted from each value of N_{CCN}/N_{CN} in AF.~~For this was corrected by subtracting the multiply charged particle fraction as determined from the D-MPSS measurements from each value of N_{CCN}/N_{CN} in AF.~~ The PNSD from the D-MPSS measurements (5 to 800 nm) are needed as the DMA-CCNC size range does not cover the large particle fraction, which is essential for the correction. Subsequently, we obtained the corrected AF curves.

Each corrected AF curve was fitted with a sigmoid function,

$$AF = \mathrm{a} + \mathrm{b}/\left(1 + \exp\left(-\frac{D_p - D_c}{\sigma_s}\right)\right) \quad (1)$$

where a is the offset from 0 in the y direction and b is the height of the upper plateau of the sigmoidal function, D_c is the critical diameter, and σ_s is a measure for the width of the sigmoid function.~~where a and b are the lower and upper limits for calculating critical diameters (D_c) at the set nominal SS, and σ_s is a measure for the width of the sigmoid function.~~ This AF fit was multiplied with the PNSD to gain the CCN number size distribution and by integrating the total number of CCN, i.e., N_{CCN}.

The critical diameter (D_c) of dry particles, κ, and mixing state at each *SS* condition can be derived from the AF fit results. Affected by aerosol mixing, the AF rises gradually from 0 to the max (~1) rather than displaying an intermittent mutation. D_c is defined as the diameter of the dry particles from which 50% of the particles are activated at the given *SS*.

The shape of the AF curve, i.e., the relative width of the AF, represents the degree of external mixture, which can be quantified by the ratio of $(D_{75} - D_{25})/D_c$ (Jurányi et al., 2013). D_{75} and D_{25} are the diameters at which 75% and 25% of the particles are activated at the given *SS*. Internal mixture implies that all particles with any given ~~equal~~ dry size have equal κ with $(D_{75} - D_{25})/D_c = 0$, whereas a distribution of different κ at a given particle size can be observed for externally mixed aerosol with higher $(D_{75} - D_{25})/D_c$ values. Note that the particle composition varying at different sizes is not defined as external mixing in this study. Jurányi et al. (2013) confirmed the reliability of this approach by comparing the κ distributions derived from parallel monodisperse CCN measurements and HTDMA measurements.

According to the derivation of κ-Köhler theory (Petters and Kreidenweis, 2007), the κ can be calculated from D_c at a given *SS*:

$$\kappa = \frac{4A^3}{27{D_c}^3 \ln^2(1 + SS/100)} \tag{2a}$$

with

$$A = \frac{4\sigma_{s/a} M_w}{RT\rho_w} \tag{2b}$$

where $\sigma_{s/a}$ is the droplet surface tension (assumed to be that of pure water, 0.0728 Nm^{-2}), M_w the molecular weight of water, R the universal gas constant, T the absolute temperature, ρ_w the density of water, and A can be considered a function of T. Thus, the

size-resolved κ (pair of κ and D_c) can be obtained at each *SS* cycle. Our monodisperse CCN measurements provide the size-resolved κ within D_p (D_c) of ~40−200 nm, which depends largely on the *SS* setting of 0.1% to 0.7%. Note that equation 2a is an approximation of κ-Köhler equation and when κ is less than 0.2, it causes a slight bias in calculating κ (Petters and Kreidenweis, 2007). Additionally, the debate about the importance of $\sigma_{s/a}$ changes and the connected bulk/surface partitioning on activation of aerosols is on ongoing (e.g., Ovadnevaite et al., 2017; Vepsäläinen et al., 2022), which is not focused on in this study.

Besides deriving it from the monodisperse CCN measurements, κ can be ~~determined~~ derived from the ACSM and MAAP chemical composition measurements (κ_{chem}) using the Zdanovskii–Stokes–Robinson (ZSR) mixing rule (Zdanovskii, 1948; Stokes and Robinson, 1966) combined with κ-Köhler theory:

$$\kappa_{chem} = \sum_i \varepsilon_i \kappa_i \tag{3}$$

where κ_i and ε_i mean the κ and volume fraction for each component, respectively, and i is the number of the component in the mixture. The ε_i was derived from its measured component i mass concentration and density (ρ_i). A simple ion-pairing scheme (Gysel et al., 2007) was used in this study with the κ_i and ρ_i values listed in Table 1 (Wu et al., 2015). ~~Note that a~~A κ of 0.1 is used for particulate organics (Dusek et al., 2010; Gunthe et al., 2009, 2011).~~;~~ F~~f~~or black carbon, we use a κ of 0 (Rose et al., 2011; Schmale et al., 2018).

The CCN number size distribution is a part of the particle number size distribution (PNSD), which approximately corresponds to the part of PNSD with $D_p > D_c$ when assuming particles to be internally mixed (Figure S2 in SI). The assumption of the internal mixing could be reasonable because the median values of the parameter b and

$(D_{75} - D_{25})/D_c$ are 1.0 and 0.18. Thus, D_c plays a critical role on diagnosing N_{CCN} in models, which can be derived from κ parameterization at a given *SS*. When κ is obtained, $D_c(\kappa, SS)$ is calculated from equation 2a. ~~When κ is given, we can predict the N_{CCN} at each *SS*. Thereto, $D_c(\kappa, SS)$ is calculated from equation 2a.~~ And, assuming an internal mixture, the predicted N_{CCN} is the integration of the PNSD from D_c, that is,

$$Predicted\ N_{CCN} = \int_{D_c}^{800} PNSD(D_p)dD_p \tag{4}$$

3. Results

3.1 Aerosol activation characteristics

As *SS* increases, the CCN number size distribution broadens towards smaller particle sizes (Figure S3 in SI), causing an increase in N_{CCN} and activation ratio (AR, i.e., ratio of N_{CCN} to total aerosol number concentration with a diameter range of 10 to 800 nm, N_{aero}). At Melpitz, the median N_{CCN} and AR increases from 399 to 2144 cm^{-3} and 0.10 to 0.48 when *SS* increases from 0.1% to 0.7%. As shown in Figure 2, the N_{CCN} measured at Melpitz is slightly higher than that measured in more remote rural background stations, e.g., in Vavihill, Sweden (Fors et al., 2011), Hyytiälä, Finland (Paramonov et al., 2015), Southern Great Plains, USA (Liu and Li, 2014), Mahabaleshwar, India (Singla et al., 2017). However, compared to the N_{CCN} measured in polluted regions (e.g., Rose et al., 2010; Deng et al., 2011; Kim et al., 2014; Varghese et al., 2016), the Melpitz N_{CCN} is much lower.

Figure 3a presents the N_{CCN} vs. *SS* and AR vs. *SS* relationships at each season and all datasets at Melpitz. The two relationships are similar, and both can be fitted well with using a power-law function (Twomey, 1959). The fit was also performed with an error function (Pöhlker et al., 2018) and the fitted parameters are in the SI (Table S2). Over the whole period, the median values of the slope parameter and the coefficient in

the N_{CCN}-SS power-law fit are 2851 cm^{-3} and 0.75, respectively, which are within the range of values for continental aerosol (slope parameter of 600–3500 cm^{-3} and coefficient of 0.4–0.9) reported in Seinfeld and Pandis (2016). The slope parameters in the power-law fitting represent the sensitivity of the N_{CCN} and AR to the variation in SS, which are highest in summer and lowest in winter. The seasonal variations of N_{CCN} and AR at SS = 0.1% and 0.7% are shown in Figure 3b. In summer, the median N_{CCN} and AR are both lowest at SS = 0.1%, which contributed to the largest sensitivity of N_{CCN} and AR to SS, i.e., the largest slope parameter in the power-law fitting among the four seasons. Additionally, the shape of the PNSD contributed to explain the sensitivity of N_{CCN} and AR to SS. The PNSD in summer was steepest in the 40-200 nm size range among the four seasons (Figure S4 in SI). Thus, in summer, a small shift in D_c will change the N_{CCN} and AR much more than those in winter where the PNSD looks broader, causing the strong sensitivity of N_{CCN} and AR to SS.

To explain the seasonal variations in aerosol activation characteristics, we investigated the PNSD and chemical compositions as shown in Figure 4. In summer, affected by the frequent NPF events (Ma et al., 2015; Wang et al., 2017), the Aitken-mode particles with D_p < 100 nm accounted for the largest portion of the PNSD (Figure S4 in SI), resulting in the highest N_{aero} and the smallest geometric mean diameter ($GMD = \exp\left(\frac{\sum_i n_i \times lnD_i}{N_{aero}}\right)$) among the four seasons. Additionally, in summer, there was the lowest bulk κ_{chem} with median value of 0.24 corresponding to the highest organic mass fraction (56% of total mass), which could be related to the strong formation of the secondary organic aerosol (SOA). Therefore, the N_{CCN} and AR both kept relatively low values in summer, especially at low SS conditions (e.g., at SS = 0.1%). On the contrary in winter, the relatively low number concentration of Aitken-mode particles caused the lowest N_{aero} and the largest GMD among the four seasons, which could be owing to the

rare NPF events. Meanwhile, in winter, low temperatures favored the particulate phase of nitrate (Poulain et al., 2011), causing the highest nitrate mass fraction (31% of total mass) among the four seasons, which might explain the highest κ_{chem} (median value of 0.34). Taking all three together, the lowest N_{aero}, the largest *GMD*, as well as the highest κ_{chem}, contribute to the highest AR value in winter at each *SS* condition. The relationships between κ_{chem} and each particle component, and the correlations among seasonal median values of N_{aero}, *GMD*, and κ_{chem} are in SI (Text S1, Figures S5 and S6).

~~Figure 3a presents the time series of the mean CCN number size distribution at each *SS* condition. As *SS* increases, CCN number size distribution broadens towards smaller particle sizes, causing an increase in N_{CCN} and activation ratio (AR, i.e., ratio of N_{CCN} to total aerosol number concentration with diameter ranging from 10 to 800 nm, N_{aero}). At Melpitz, the mean N_{CCN} is 513, 1102, 1466, 2020, and 2477 cm^{-3} at *SS* of 0.1%, 0.2%, 0.3%, 0.5%, and 0.7%, respectively. The mean AR ranged from 0.11 to 0.52 at *SS* = 0.1% to 0.7%. As shown in Table 2, the mean N_{CCN} measured at Melpitz is generally higher than that measured in more remote rural background stations. For instance, as *SS* increased from 0.1% to 1.0%, the mean N_{CCN} increased from 362 to 1795 cm^{-3} in Vavihill, Sweden (Fors et al., 2011) and 274 to 1128 cm^{-3} in Hyytiälä, Finland (Paramonov et al., 2015); in Southern Great Plains, USA, the mean N_{CCN} at *SS* = 0.4% was 1248 cm^{-3} (Liu and Li, 2014); the mean N_{CCN} increased from 118 to 1826 cm^{-3} as *SS* increased from 0.1% to 0.94% in Mahabaleshwar, India (Singla et al., 2017). However, the mean N_{CCN} measured at Melpitz is far lower than that measured in polluted regions. For example, in a rural site of Guangzhou, China, the mean N_{CCN} increased from 995 to 10731 cm^{-3} as *SS* increased from 0.068% to 0.67% (Rose et al., 2010); higher N_{CCN} was observed in Wuqing, China, with the mean N_{CCN} of 2192–12963 cm^{-3} at *SS* = 0.056–0.7% (Deng et al., 2011); in an urban site of Seoul, Korea, the mean~~

~~N_{CCN} increased from 4145 to 6067 cm^{-3} as SS increased from 0.4% to 0.8% (Kim et al., 2014); in a polluted continental site of Mahabubnagar, India, the mean N_{CCN} at SS = 1.0% was ~5400 cm^{-3} (Varghese et al., 2016).~~

~~At Melpitz, aerosol activation characteristics are highly variable across seasons. At SS = 0.1%, CCN number size distribution is wider in spring and winter than in summer and autumn; the mean N_{CCN} at SS = 0.1% is 585, 347, 440, and 681 cm^{-3} in spring, summer, autumn, and winter, respectively. The mean N_{CCN} at SS = 0.1% in winter is almost twice as high as that found in summer. The highest mean AR at SS = 0.1% was 0.18 observed in winter, whereas the lowest mean AR (0.06) was observed in summer. In spring and autumn, the mean AR at SS = 0.1% is 0.1. As SS increases, CCN number size distribution gradually peaks in summer, especially at SS = 0.5% and 0.7%. At SS = 0.7%, the mean N_{CCN} is 2622, 2530, 2222, and 2495 cm^{-3}, and the mean AR is 0.49, 0.41, 0.51, and 0.68 in spring, summer, autumn, and winter, respectively.~~

~~The AR-SS and N_{CCN}-SS relationships in each season and all datasets are shown in Figures 3b and 3c. The two relationships are similar, and both can be fitted well with using the power-law function (Twomey, 1959) and the error function (Pöhlker et al., 2018). The fit results are shown in Table 3. The error function fits the relationships better than the power-law function because of more parameters. The power parameter in the power-law function means the change rate of the controlled variable with the independent variable, that is the slope in a log-log coordinate system, so it is also called the slope parameter. In the power-law fits of the two relationships, the slope parameters are highest in summer and lowest in winter. Therefore, AR and N_{CCN} are most sensitive to SS in summer, whereas the opposite is true in winter. The coefficients in the power-law fits represent the AR and N_{CCN} at SS = 1%. The coefficient in AR-SS fit is highest in winter (0.89) and lowest in summer (0.61). However, the coefficient in N_{CCN}-SS fit~~

~~is highest in summer (3951 cm^{-3}) and lowest in autumn (3136 cm^{-3}). Over the whole period, the mean values of the slope parameter and the coefficient in the N_{CCN}-SS power-law fit are 3497 cm^{-3} and 0.81, respectively, which are within the range of values for continental aerosol (slope parameter of 600–3500 cm^{-3} and coefficient of 0.4–0.9) reported in Seinfeld and Pandis (2016).~~

~~CCN number size distribution is a part of the particle number size distribution (PNSD), which approximately corresponds to the part of PNSD with $D_p > D_c$ when assuming particles to be internally mixed. The schematic diagram in Appendix A shows the relationship between the PNSD and the CCN number size distribution. Aerosol chemical composition determines the κ through equation 3, thereby changing D_c at a given SS condition through equation 2a. Thus, we present the time series of the PNSD and chemical compositions in Figure 4 to explain the variations in aerosol activation characteristics.~~

~~In summer, affected by the frequent NPF events (Ma et al., 2015; Wang et al., 2017), the Aitken-mode particles with $D_p < 100$ nm account for the largest portion of the PNSD, resulting in the highest N_{aero} with a mean value of 6224 cm^{-3} and the smallest geometric mean diameter ($GMD = \exp\left(\frac{\sum_i n_i \times \ln D_i}{N_{aero}}\right)$) with a mean value of 50 nm among the four seasons. On the contrary, in winter, the mean GMD increases to 58 nm, which is the largest among the four seasons, and the N_{aero} decreases to the lowest with a mean value of 3686 cm^{-3} because of the rare NPF events. During the NPF events, only a part of newly formed particles grows to sizes larger than D_c (e.g., ~55 nm at $SS = 0.7\%$), whereas most of the new particles are still unactivated at $SS \leq 0.5\%$. Therefore, CCN number size distribution gradually peaks as SS increases in summer, whereas AR keeps a minimum even at relatively high SS conditions as shown in Figure 3a. In winter, the lowest N_{aero} and the largest GMD contribute to the highest AR at each SS condition.~~

~~Figure 4b shows the average changes of the aerosol particle chemical compositions over a year and the estimated bulk κ_{chem} of submicron aerosol particles. At Melpitz, the mean value of bulk κ_{chem} is 0.36 with one standard deviation of 0.09 over the whole period; the seasonal mean κ_{chem} plus/minus one standard deviation are 0.38±0.09, 0.29±0.08, 0.36±0.08, and 0.40±0.08 in spring, summer, autumn, and winter, respectively. Because the κ_{chem} depends on aerosol particle chemical composition through equation 3, we examined the correlation between κ_{chem} and the mass fraction of each component to explain the variations of κ_{chem}. As shown in Figures 5a and 5b, a negative correlation between the κ_{chem} and the organic mass fraction (f_{org}) was observed, while an opposite trend was found for the nitrate ($f_{nitrate}$). Additionally, the κ_{chem} is not correlated with the sulfate mass fraction ($f_{sulfate}$) and the BC mass fraction (f_{BC}), as shown in Figures 5c and 5d.~~

~~In summer, there is the lowest bulk κ_{chem} with 0.29±0.08 corresponding to the highest f_{org} (56% of total mass on average), which could be related to the strong formation of the secondary organic aerosol. In winter, low temperatures favor the particulate phase of nitrate (Poulain et al., 2011) with a mean $f_{nitrate}$ of 31%, which might explain the highest κ_{chem} (0.40±0.08). According to equation 2a, D_c increases as κ decreases at a given SS condition. Thus, the lowest κ_{chem} results in the narrowest CCN number size distribution and a decrease in N_{CCN} in summer, especially at relatively low SS conditions (e.g., 0.1% and 0.2%) as shown in Figure 3a.~~

3.2 Size-resolved particle hygroscopicity factor and mixing state

The hygroscopicity factor and the mixing state directly influence the D_c and the shape of the AF curve, thereby changing the N_{CCN} at a given SS condition. Affected by the variations of particle composition, t~~T~~hese two parameters are not constant and both

vary with particle size and season.

Figure ~~6a~~ 5a presents monthly median values of κ_{chem} ~~monthly averages of~~ and κ calculated from monodisperse CCN measurements (κ_{CCN}) at *SS* of 0.1% and 0.7%. Their ~~each *SS* condition, and their~~ seasonal ~~mean~~ median values are summarized in Table ~~4~~2. At Melpitz, the median κ_{CCN} decreased from 0.27 to 0.19 as *SS* increased from 0.1% to 0.7%, which was less than the median bulk κ_{chem} of 0.3. The seasonal variation of κ_{CCN} at *SS* of 0.1% is similar to that of κ_{chem}, whereas the seasonal trend in κ_{CCN} is much weaker at *SS* = 0.7%. Essentially, the relationship between κ_{CCN} and *SS* is determined by the κ_{CCN} vs. D_p relationship. The κ_{CCN} at *SS* of 0.1% and 0.7% correspond to the median D_c (i.e., D_p) of 176 and 54 nm, respectively. As the ACSM is sensitive to particle mass rather than number concentration, the bulk composition is dominated by the contribution of the larger particles. In the median volume size distribution of particle, the peak diameter was at ~300 nm (Poulain et al., 2020). Thus, κ_{chem} may be representative for the larger particles rather than for the smaller particles. Owing to the positive correlation between κ and D_p (Figure 6a), the κ_{chem} representing for the larger particles could be greater than the κ_{CCN} for the smaller particles. Figure 5b depicts the monthly variation of D_c at *SS* of 0.1% and 0.7%, which shows the opposite trend to $\kappa_{CCN}(SS)$ because of the negative correlation of $D_c^3(SS)$ vs. $\kappa(SS)$ shown in equation 2a. Compared to the D_c at lower *SS* conditions (e.g., 0.1%), D_c has a more significant seasonal trend at higher *SS* conditions (e.g., 0.7%). At *SS* = 0.7%, the low κ_{CCN} caused the large D_c in summer, whereas the high κ_{CCN} caused the small D_c in spring and winter.

~~At Melpitz, the mean κ_{CCN} plus/minus one standard deviation over all datasets are 0.28±0.08, 0.28±0.10, 0.24±0.10, 0.21±0.09, and 0.20±0.09 at *SS* = 0.1%, 0.2%,~~

~~0.3%, 0.5%, and 0.7%, respectively, where the mean κ_{CCN} were all less than the mean bulk κ_{chem} of 0.36. The seasonal variation of κ_{CCN} at each *SS* condition is similar to that of κ_{chem}. In summer, κ_{CCN} is lowest among the four seasons, with mean values of 0.23, 0.25, 0.21, 0.19, and 0.19 at *SS* = 0.1%, 0.2%, 0.3%, 0.5%, and 0.7%, respectively. The highest κ_{CCN} at each *SS* condition was observed in winter, with mean values of 0.32, 0.32, 0.28, 0.23, and 0.21 at *SS* = 0.1%, 0.2%, 0.3%, 0.5%, and 0.7%, respectively. κ_{CCN} in spring are slightly lower than that in winter, with mean values of 0.31, 0.32, 0.27, 0.22, and 0.21 at *SS* = 0.1%, 0.2%, 0.3%, 0.5%, and 0.7%, respectively. In autumn, the mean κ_{CCN} are 0.27, 0.26, 0.22, 0.19, and 0.19 at *SS* = 0.1%, 0.2%, 0.3%, 0.5%, and 0.7%, respectively, which is slightly higher than that observed in summer.~~

~~Figure 6b presents the monthly variation of D_e at each *SS* condition, which shows the opposite trend to κ_{CCN} – *SS* because of the negative correlation of D_e^3 vs. κ shown in equation 2a. The seasonal mean D_e are shown in Table 4. The mean D_e plus/minus one standard deviation over the whole period are 177±19, 112±14, 91±15, 67±9, and 54±8 nm at *SS* = 0.1%, 0.2%, 0.3%, 0.5%, and 0.7%, respectively. The largest D_e at each *SS* condition were observed in summer, with mean values of 187, 116, 94, 69, and 55 nm at *SS* = 0.1%, 0.2%, 0.3%, 0.5%, and 0.7%, respectively. Followed by autumn and spring, the smallest D_e at each *SS* condition was observed in winter, with mean values of 168, 107, 86, 64, and 53 nm at *SS* = 0.1%, 0.2%, 0.3%, 0.5%, and 0.7%, respectively.~~

The monthly ~~average~~ trend of the external-mixing degree $((D_{75} - D_{25})/D_c)$ is shown in Figure ~~6c~~5c. ~~The degree of external mixture is quantified by the ratio of $(D_{75} - D_{25})/D_e$. The seasonal mean $(D_{75} - D_{25})/D_e$ are presented in Table 4.~~ Jurányi et al. (2013) pointed out that the $(D_{75} - D_{25})/D_c$ ranged from 0.08 to 0.12 for ammonium sulfate calibration measurements at *SS* = 0.1−1.0%, which indicated an internal mixture within

measurement accuracy. For our measurements, the median~~mean~~ $(D_{75} - D_{25})/D_c$ over all datasets range from 0.~~17~~ 15 to 0.~~25~~ 20 at SS = 0.1−0.7%. The median $(D_{75} - D_{25})/D_c$ was low in summer and spring and high in winter and autumn. The results tend to indicate that the aerosol particles at Melpitz were more internally mixed in summer and spring whereas less internally mixed in winter and autumn.~~In summer, $(D_{75} - D_{25})/D_e$ is lowest ranging from 0.14 to 0.18 at SS = 0.1−0.7%, implying that aerosol particles were extremely close to being internally mixed. Followed by spring and autumn, the highest $(D_{75} - D_{25})/D_e$ was observed in winter with values ranging from 0.24 to 0.36 at SS = 0.1−0.7%. Therefore, the results tend to indicate that the aerosol particles were less internally mixed in winter among the four seasons at Melpitz. In non-urban location~~ In summer, the less contribution from anthropogenic emissions and the faster aging process as well as SOA formation caused by atmospheric chemistry certainly contribute to make particles more internally mixed. Changes in organic aerosol (OA) composition can be found in Crippa et al. (2014), Poulain et al. (2014), and Chen et al. (2022). In cold seasons, the local pollution (100 km around) is dominated by liquid fuel, biomass, and coal combustions mostly for house heating (van Pinxteren et al., 2016). During winter long-range transport from the eastern wind bring to the station continental air masses which are strongly influence by anthropogenic emissions (in opposition to western marine air masses). These particles are a mixture of different anthropogenic sources emitted all along the transport as well as including some local and regional sources (most house heating). All of them at different aging state cause the overall particles more externally mixed. ~~s, initially externally mixed aerosol particles become an internal mixture on a time scale of ~1 day (Fierce et al., 2016). In winter, the relatively stable weather patterns increase the persistence of aerosol (> 5 days) at Melpitz (Schmale et al., 2018). When tracking an aerosol cluster, the prolonged mixing~~

~~time should promote the aging process, leading to an internal mixture. However, we observed a less internally mixed aerosol particle population in winter. A plausible explanation is mixing in of local pollution.~~

As mentioned above, κ_{CCN} (and $(D_{75} - D_{25})/D_c$) vs. D_p relationships determine the relationship between κ_{CCN} (and $(D_{75} - D_{25})/D_c$) and *SS*. Monodisperse CCN measurements provide the size-resolved κ and $(D_{75} - D_{25})/D_c$. At a given *SS* condition, κ_{CCN} represents the κ of particles at $D_p = D_c$, and the same is true for $(D_{75} - D_{25})/D_c$. ~~Essentially, the relationship between κ_{CCN} and *SS* is determined by the κ_{CCN} vs. D_p relationship. Identically, the relationship between $(D_{75} - D_{25})/D_e$ and *SS* depends on the $(D_{75} - D_{25})/D_e$ vs. D_p relationship. Monodisperse CCN measurements provide the size-resolved κ and $(D_{75} - D_{25})/D_e$. At a given *SS* condition, κ_{CCN} represents the κ of particles at $D_p = D_e$, and the same is true for $(D_{75} - D_{25})/D_e$. It should be noted that our monodisperse CCN measurements only provide the size-resolved κ and $(D_{75} - D_{25})/D_e$ within D_p of ~40–200 nm.~~ As shown in Figure ~~7a~~6a, κ_{CCN} increases with D_p at D_p range of ~40 to 100 nm, whereas κ_{CCN} almost stays constant at D_p of 100 to 200 nm for all seasons. Additionally, the increase κ_{CCN} with D_p varies with season. The κ_{CCN} vs. D_p relationship is fitted by a power-law function at each season. ~~Fit results are presented in Table 5.~~ In summer, there is the lowest slope parameter ~~of 0.19~~ in the κ_{CCN} vs. D_p power-law fit, meaning that the κ_{CCN} is least sensitive to D_p. Compared to the cold seasons, the anthropogenic emissions linked to house heating strongly reduce in summer which affect the smaller particles, and the dominant small particles ($D_p < 100$ nm) are associated to NPF and the SOA formation. NPF is a complex process which depends on the availability of condensing material (H_2SO_4 and organic), as well as pre-existing particles (coagulation and condensation sink parameters). Therefore, same

condensing material on the gas phase can either condense on pre-existing particles (usually larger than 100 nm and then detected by ACSM) or lead to NPF formation. A direct consequence of it is a probable smaller effect of the size dependent chemical composition of the particles. This might explain why κ_{CCN} at *SS* of 0.1% and 0.7 % are closer, i.e., the weaker sensitive of κ_{CCN} to D_p in summer.~~meaning that the difference between the κ_{CCN} at different particle sizes is smallest among the four seasons. Followed by autumn with the slope parameter of 0.31, the slope parameter is highest in spring and winter of 0.36–0.37. Therefore, the κ_{CCN} is most sensitive to D_p in spring and winter.~~ Figure ~~7b~~ 6b presents the $(D_{75} - D_{25})/D_c$ vs. D_p relationship. As particle size increases, $(D_{75} - D_{25})/D_c$ decreases at D_p of ~40 to 200 nm for all seasons, meaning that small particles are less internally mixed. The reason is that during the aerosol aging process, not only particle size increases but κ becomes more uniform. The $(D_{75} - D_{25})/D_c$ vs. D_p relationship is also fitted well by ~~the~~ a power-law function at each season~~, with fit results shown in Table 5~~. The lowest absolute value of the slope parameter was observed in summer, indicating that the degree of external mixture was least sensitive to D_p, which could be related to the less mixing between the local emissions and long-range transport particles in summer. ~~The highest absolute value of the slope parameter was observed in autumn of 0.42, followed by winter of 0.30 and spring of 0.26, and the lowest was 0.20 observed in summer. Thus, the difference between the degree of external mixture at different particle sizes is largest in autumn, followed by winter and spring, and is smallest in summer.~~

3.3 N_{CCN} prediction at Melpitz

N_{CCN} plays an important role in modeling the formation and evolution of clouds ~~(Zhao et al., 2012; Fan et al., 2012, 2018)~~. In t~~T~~his section, we evaluate~~s~~ the accuracy of N_{CCN} predicted from five ~~different~~ schemes. Table ~~6~~ 3 introduces the five schemes,

which can be summarized into two categories~~ of N_{CCN} prediction approach~~. From polydisperse CCN measurements, the N_{CCN} (AR) and *SS* relationships can be obtained, and their fitting results can be used to predict N_{CCN} at the given *SS* conditions, which belongs to the 1st category, corresponding to the N1 and N2 schemes in Table 3, respectively.~~The fit results of N_{CCN} – *SS* relationship and *AR* - *SS* relationship can predict N_{CCN} at the given *SS* conditions, which belongs to the 1st category approach, corresponding to the 1st and 2nd schemes in Table 6, respectively.~~ Compared to CCN measurements, it is generally more common and simpler to obtain the PNSD measurements.~~;~~ T~~t~~hus, we usually predict N_{CCN} using the real-time PNSD combined with the parameterized $\kappa(D_c)$~~CCN activity~~, which belongs to the 2nd category~~ approach~~. The 2nd category includes the last three schemes (K1, K2, and K3) in Table 3, but they vary in assuming κ. ~~The last three schemes in Table 6 belong to the 2nd category approach, but they vary in assuming κ.~~ The ~~3rd~~ K1 scheme uses a fixed κ of 0.3 without temporal and size-dependent variations, as recommended for continental aerosol (Andreae and Rosenfeld., 2008), which is also the median value of κ_{chem} over all data setting at Melpitz. The ~~4th~~ K2 scheme uses the bulk κ_{chem} calculated from aerosol chemical composition, which is also non-size-dependent but changes over time. The ~~5th~~ K3 scheme uses the κ - D_p power-law fit results shown in ~~Table 5~~Figure 6a, which are size-dependent without temporal variations at each season. Applying the κ - D_p power-law equation into equation 2a, D_c can be derived as function of *SS*,

$$D_c = \left(\frac{4 \times A^3}{27 \times coef \times \ln^2(1 + SS/100)}\right)^{\frac{1}{slope+3}} \tag{5}$$

where the *slope* and *coef* represent the slope parameter and the coefficient in κ - D_p power-law fit. Subsequently, the predicted N_{CCN} can be calculated through equation 4. The 2nd category~~last three schemes all~~ assumed that aerosol particles are internally

mixed at a particular D_p, as used in many previous N_{CCN} prediction studies (e.g., Deng et al., 2013; Pöhlker et al., 2016; Wang et al., 2018a).

The prediction results are shown in Figure ~~8~~7. The linear equation (y = kx) is used to fit the relationship between the predicted N_{CCN} and the measured one, and its slope represents the mean ratio of the predicted N_{CCN} to the measured N_{CCN}. ~~To make the results of the predictions comparable for all regression schemes, we also applied a linear regression to the 1st scheme and forced the linear regression through zero for all schemes.~~ The relative deviation (RD) equals the ratio of the absolute difference between the predicted N_{CCN} and the measured one to the measured N_{CCN},

$$RD = \frac{|predicted\ N_{CCN} - measured\ N_{CCN}|}{measured\ N_{CCN}}. \quad (6)$$

The median RD was used to quantify the deviation between predictions and measurements of each scheme. The slope and median RD shown in Figure 7 are both calculated from all five *SS* conditions for each season. As shown in Figure 7, the N1 and N2 schemes only provide rough estimates of the N_{CCN} which is reflected in the high median RD. The results for N1 and N2 schemes are similar in that they both predict the overall mean N_{CCN} well (slopes of approximately 1.0) but with large median RDs. Compared to N1 scheme, the N2 scheme is better because of the lower median RD. Compared to the 1st category (the N1 and N2 schemes), the 2nd category (the K1, K2, and K3 schemes) predicts N_{CCN} better because of the lower median RD. The results for K1 and K2 are similar in that they both overestimate N_{CCN} by approximately 10% (slopes of approximately 1.1) with similar median RDs. The reason for the N_{CCN} overestimation is that the constant κ of 0.3 and the real-time bulk κ_{chem} are both greater than the κ_{CCN} at each season. In winter, the κ_{CCN} was highest and the difference between the κ_{CCN} and the parameterized κ in K1 and K2 scheme was lowest, causing the best

prediction of N_{CCN} among the four seasons. Owing to the largest difference between the κ_{CCN} and the parameterized κ, the N_{CCN} prediction was worst in summer for K1 scheme and in autumn for K2 scheme. The K3 scheme appears to be the best one for N_{CCN} prediction among the five schemes which is reflected in the lowest median RDs and the fit slope of ~1.0 for different seasons. The evaluations of the five schemes for the N_{CCN} prediction at each *SS* condition and each season are provided in Figure S7 in SI.~~–i.e., RD = (|predicted N_{CCN} – measured N_{CCN}|)/measured N_{CCN}; a large RD represents a large deviation between prediction and measurement. The slope and RD shown in Figure 8 are both calculated from all five *SS* conditions for each season. As shown in Figure 8, the 1st and 2nd schemes only provide rough estimates of the N_{CCN} on account of the pretty high RD ranging from 64% to 136%. Compared to the 1st category approach (the 1st and 2nd schemes), the 2nd category approach (the 3rd, 4th, and 5th schemes) predicts N_{CCN} better. The predicted N_{CCN} correlates well with the measured one for the 3rd, 4th, and 5th schemes with $R^2 > 0.97$; but N_{CCN} is generally overestimated for the 3rd and 4th schemes because the fit slopes range from 1.03 to 1.17 for different seasons. The 5th scheme appears to be the best one for N_{CCN} prediction among the five schemes on account of the lowest RD ranging from 11% to 17% and the fit slope of ~1 for different seasons. It should be noted that the fit slope shown in Figure 8 represents the average over all five *SS* conditions, which could obscure the performance at each *SS* condition. Thus, Figure 9 further evaluates the five schemes for the N_{CCN} prediction at each *SS* condition.~~

The K3 scheme provides an improved prediction of N_{CCN}, which is obvious when compared to N1 and N2 schemes. Compared to K1 and K2 schemes, the K3 scheme reduced approximately 10% overestimation of N_{CCN} because the fitting slope decreased ~0.1 on average. We simply evaluate the effects of the 10% overestimation in N_{CCN} on

predictions of cloud radiative forcing and precipitation. The methods are in Text S2 in SI and Wang et al. (2019). Essentially, an overestimation of N_{CCN} leads to overestimate the number concentration of cloud droplet (N_C) in models. Theoretically, it can reduce 3.2% overestimation of cloud optical thickness, corresponding to global average difference of 1.28 Wm^{-2} when assuming the cloud shortwave cooling effect of 40 Wm^{-2} (Lee et al., 1997), which amounts to approximately one-third of the direct radiative forcing from a doubling CO_2. Additionally, the overestimation in N_{CCN} (and N_C) leads to underestimate the strength of the autoconversion process in cloud (Liu et al., 2006), thereby suppressing precipitation. Therefore, although ACSM measurements can derive κ_{chem} and thus predict N_{CCN}, the monodisperse CCN measurements are still important to obtain the κ - D_p relationship and thus improve the predictions of N_{CCN} (and N_C) and climate.

Figure 8 compared the κ - D_p relationship measured at different regions. The κ - D_p relationship measured at Melpitz is similar to that measured at other rural regions with similar κ - D_p power-law fitting results, e.g., the Vavihill station in Sweden (Fors et al., 2011) and the Xinken station in China (Eichler et al., 2008). Therefore, the κ - D_p power-law fit measured at Melpitz could be applied to predict N_{CCN} for these rural regions. However, it may cause considerable deviations for different aerosol background regions, e.g., the suburb stations in Xingtai, China (Wang et al., 2018a) and in Paris, France (Mazoyer et al., 2019), the coast of Barbados (Kristensen et al., 2016), the amazon rainforest (Pöhlker et al., 2016), and the urban stations in Budapest, Hungary (Salma et al., 2021) and in Shanghai, China (Ye et al., 2013), because their κ - D_p relationships are different from that measured at Melpitz.

~~When using the N_{CCN} – SS power-law fit (the 1st scheme) to predict N_{CCN}, it causes significant overestimations of N_{CCN} at SS = 0.1% with median values ranging from 3%~~

~~to 29% for different seasons and causes less than 21% underestimations in median at other larger *SS* conditions. Additionally, the prediction results are much uncertain at a given *SS* condition and season, especially at *SS* = 0.1%. For instance, one-quarter of the predicted N_{CCN} are twice higher than the measured values at *SS* = 0.1% for all datasets. Thus, this scheme can only be used to provide rough estimations of N_{CCN}.~~

~~When using the real-time N_{aero} combined with *AR* – *SS* power-law fit (the 2nd scheme) to predict N_{CCN}, the performances are slightly better than those of the 1st scheme. The median overestimations of N_{CCN} are less than 17% at *SS* = 0.1% for all seasons, while the median underestimations of N_{CCN} range from 12% to 35% at *SS* = 0.2%–0.7% for all seasons. Similarly, the prediction results remain a high uncertainty at a given *SS* condition and season. Thus, this scheme also provides rough estimations on N_{CCN}.~~

~~When assuming the real-time PNSD combined with a constant κ of 0.3 (the 3rd scheme) to predict N_{CCN}, it causes overestimations of N_{CCN} in most cases. The median of the overestimation ranges from -3% to 30% at *SS* = 0.1%–0.7% for different seasons. As shown in Figure 7a, a constant κ of 0.3 is almost greater than the κ_{CCN} of all particles with the diameter ranging from ~40 to 200 nm, except for the accumulation-mode particles (D_p of 100 to 200 nm) in spring and winter. Therefore, besides the well-predicted N_{CCN} at *SS* = 0.1% and 0.2% in spring and winter, N_{CCN} is overestimated at assuming a constant κ of 0.3 as shown in Figure 9c. The largest overestimation occurs at *SS* = 0.1% in summer (30% in median) because of the low κ_{CCN} (0.22 in average) combined with the low measured N_{CCN} (347 cm^{-3} in average). Although the largest median overestimation reaches to 30%, which is numerically similar to the largest median overestimation of the 1st scheme (29%) and the largest median underestimation of the 2nd scheme (35%), the uncertainties of the 3rd scheme are much lower than those~~

~~of the 1st and 2nd schemes. For example, when using 3rd scheme, one-quarter of the ratio of the predicted N_{CCN} to the measured N_{CCN} are larger than 1.31 at SS = 0.1% for all datasets as shown in Figure 9c, while the ratio is ~2.0 for both the results of 1st and 2nd scheme as shown in Figures 9a and 9b. Thus, the 3rd scheme has better predictions on N_{CCN} compared to the 1st and 2nd schemes.~~

~~When assuming the real-time PNSD combined with the real-time bulk κ_{chem} (the 4th scheme) to predict N_{CCN}, it also causes clear overestimations of N_{CCN} in most cases, like the prediction results calculated from the 3rd scheme. The median overestimations are within 7% to 21% at SS = 0.1%–0.7% for different seasons. The reason for the overestimation is that the κ_{chem} is greater than κ_{CCN} measured at all the five SS conditions. For instance, the mean κ_{CCN} over all datasets ranges from 0.20 to 0.28 at SS = 0.1%–0.7%, whereas the mean κ_{chem} over all datasets is 0.36. The largest overestimation also occurs at SS = 0.1% in summer with 21% in median. Compared to the 3rd scheme, the uncertainty of the N_{CCN} prediction at a given SS condition and season is lower in the 4th scheme. Considering the median overestimations of the predicted N_{CCN} at different seasons and SS conditions and the uncertainty of the predicted N_{CCN} at each given season and SS condition, we conclude that the performances of the 4th scheme are better than the 3rd scheme.~~

~~When assuming the real-time PNSD combined with the κ - D_p power-law fit (the 5th scheme) to predict N_{CCN}, it can predict the N_{CCN} well at each SS condition for all seasons. At SS = 0.1%, it causes less than 10% overestimation in median for N_{CCN} prediction for all seasons; at SS = 0.2%–0.7%, the median overestimation ranges from -3% to 6% for all seasons. The uncertainty of the N_{CCN} prediction at a given SS condition and season is also smallest among the five schemes, especially at relatively high SS conditions (e.g., 0.5% and 0.7%). For instance, at SS = 0.7% for all datasets, when using~~

~~the 5th scheme, one-quarter of the ratio of the predicted N_{CCN} to the measured N_{CCN} are larger than 1.10, while the ratio ranges from 1.18 to 1.38 for other four schemes. Therefore, the 5th scheme provides the best N_{CCN} prediction among the five schemes.~~

~~Overall, the performance for N_{CCN} prediction is gradually getting better from the 1st to the 5th scheme shown in Table 6. The classic N_{CCN} – SS and AR - SS power-law fits shown in Table 3 can only be used to provide rough estimates of the N_{CCN}. At Melpitz, using a constant κ of 0.3 or the bulk κ_{chem} both causes significant overestimations of N_{CCN} with about 30% in median, especially at SS = 0.1% in summer. The κ - D_p power-law fit at each season shown in Table 5 is recommended applying for N_{CCN} prediction at Melpitz, which can narrow down the prediction deviation (ratio of the predicted N_{CCN} to the measured N_{CCN} minus 1) within 10% in median. Additionally, as shown in Figure 10, the κ - D_p power-law fit measured at Melpitz is similar to that measured at other rural and continental regions with similar aerosol background conditions, e.g., the Vavihill station in Sweden (Fors et al., 2011) and the Xinken station in China (Eichler et al., 2008), and is also valid for some urban (Ye et al., 2013) and suburb regions (Mazoyer et al., 2019). Therefore, the κ - D_p power-law fit measured at Melpitz could be applied to predict N_{CCN} for these regions. However, it may cause considerable deviations for different aerosol background regions, e.g., the polluted suburb station in Xingtai, China (Wang et al., 2018a), the coast of Barbados (Kristensen et al., 2016), the amazon rainforest (Pöhlker et al., 2016), and the urban station in Budapest, Hungary (Salma et al., 2021), because their κ - D_p relationships are different from that measured at Melpitz.~~

~~Additionally, it should be noted that the main size dependence of κ occurs at D_p of ~40 to 100 nm as shown in Figure 7a, which would be for SS larger than 0.2%. At D_p of 100 to 200 nm corresponding to SS less than 0.2%, κ almost stays constant. The mean~~

~~value of κ is close to 0.3 for spring and winter, and that's where deviations in Figure 9c are small. However, the mean value of κ overestimates the κ for SS larger than 0.2% at each season. We further compare the N_{CCN} predictions between using the seasonally mean value of κ over D_p of 100 to 200 nm and the κ - D_p power-law fit. As shown in Figure 11, at SS = 0.1 and 0.2%, the seasonally mean κ value over D_p of 100 to 200 nm and κ - D_p power-law fit both predict the N_{CCN} well at each season, while the mean κ value leads to significant overestimation of N_{CCN} within 10% on average at SS = 0.3, 0.5, and 0.7%. Therefore, to predict the N_{CCN} at a relatively low SS of less than 0.2% (e.g., in fog and shallow stratiform cloud), the mean κ value over D_p of 100 to 200 nm also works well. The mean value plus/minus one standard deviation are 0.32±0.09, 0.24±0.07, 0.26±0.09, 0.32±0.10 and 0.28±0.09 for spring, summer, autumn, winter, and all datasets, respectively.~~

4. Conclusions

Aerosol particle activation plays an important role in determining N_C~~the number concentration of cloud droplets~~, thereby affecting cloud microphysics, precipitation processes, radiation, and climate. To reduce the uncertainties and gain more confidence in the simulations on AIEs, long-term measurements ~~on~~ of aerosol activation characteristics are essential~~;~~. H~~h~~owever, they are still rarely reported. Based on more than 4-year comprehensive measurements conducted at the central European ACTRIS site Melpitz, Germany, this study presents a systematic seasonal analysis of aerosol activation characteristics and N_{CCN} predictions.

Over the whole period at Melpitz, the ~~mean~~ median N_{CCN} and AR increased from 399 to 2144 cm^{-3} and 0.10 to 0.48~~513 to 2477 cm^{-3} and 0.11 to 0.52~~ with SS increasing from 0.1% to 0.7%, respectively. Aerosol activation characteristics are highly variable across seasons, especially at relatively low SS conditions. For instance at SS = 0.1%,

the median N_{CCN} and AR in winter are 1.6 and 2.3 times higher than the summer values, respectively. Aerosol particle activation depends on its physical and chemical properties. In summer, the highest N_{aero}, smallest *GMD*, steepest PNSD in 40-200 nm size range, and lowest κ_{chem} all contribute to the lowest AR and N_{CCN} among the four seasons, and the reverse holds true in winter.

~~At *SS* = 0.1%, the seasonal mean N_{CCN} is 681 cm^{-3} in winter, which is almost twice higher than the summer value (347 cm^{-3}); the seasonal mean AR is 0.18 in winter, which is three times higher than the summer value (0.06). Aerosol particle activation depends on its physical and chemical properties. Affected by the frequent NPF events, in summer, the mean N_{aero} is highest (6224 cm^{-3}) and the mean *GMD* is smallest (50 nm) among the four seasons. On the contrary in winter, the mean N_{aero} is lowest (3686 cm^{-3}) and the mean *GMD* is largest (58 nm). In summer, the mean f_{org} (56%) is highest among the four seasons, corresponding to the lowest κ_{chem} with a mean value of 0.29; in winter, the mean $f_{nitrate}$ (36%) is highest among the four seasons, which might explain the highest mean κ_{chem} (0.40). Therefore, in winter, the highest κ_{chem}, largest *GMD*, and the lowest N_{aero} cause the highest AR at each *SS* condition among the four seasons.~~

Both κ and the mixing state are size-dependent, thereby varying with *SS*. The median κ_{CCN} decreases from 0.27 to 0.19 as *SS* increases from 0.1% to 0.7%, which was less than the median bulk κ_{chem}. ~~The mean κ is 0.28, 0.28, 0.24, 0.21, and 0.20 at *SS* = 0.1%, 0.2%, 0.3%, 0.5%, and 0.7%, respectively. D_e depends on κ at a given *SS* conditio~~The seasonal trend of κ_{CCN} was similar to that of κ_{chem}, especially at relatively low *SS* conditions. The lowest κ_{CCN} and κ_{chem} were observed in summer, which related to the highest organics mass fraction in particles. Aerosol particles were more internally mixed in summer and spring whereas less internally mixed in winter and autumn. In cold seasons, the increasing anthropogenic emissions linked to house heating mixed

with the aged particles from long-range transport, which could decrease the degree of internal mixing of particles. As D_p increases, κ_{CCN} increases at D_p range of ~40 to 100 nm and almost stays constant at D_p range of 100 to 200 nm, whereas the $(D_{75} - D_{25})/D_c$ monotonically decreases. The relationships of $(D_{75} - D_{25})/D_c$ vs. D_p and κ vs. D_p are both fitted well by a power-law function for each season.

~~The mean D_c is 177, 112, 91, 67, and 54 nm at SS = 0.1%, 0.2%, 0.3%, 0.5%, and 0.7%, respectively. For different seasons, the seasonal mean κ varies from 0.23 to 0.32 at SS = 0.1%, and 0.19 to 0.21 at SS = 0.7%; the seasonal mean D_c varies from 168 nm to 187 nm at SS = 0.1%, and 53 nm to 55 nm at SS = 0.7%. The degree of external mixture is quantified by the $(D_{75} - D_{25})/D_c$, which ranges from 0.17 to 0.25 in average over the whole period at SS = 0.1–0.7%. In summer, aerosol particles were extremely close to being internally mixed with $(D_{75} - D_{25})/D_c$ ranging from 0.14 to 0.18 at SS = 0.1–0.7%; in winter, particles were less internally mixed among the four seasons with $(D_{75} - D_{25})/D_c$ ranging from 0.24 to 0.36 at SS = 0.1–0.7%. As D_p increases, κ increases at D_p of ~40 to 100 nm and almost stays constant at D_p of 100 to 200 nm), and $(D_{75} - D_{25})/D_c$ decreases for all seasons. The relationships of $(D_{75} - D_{25})/D_c$ vs. D_p and κ vs. D_p are both fitted well by the power-law function for each season.~~

Five activation schemes are evaluated on the N_{CCN} predictions. Compared to using the classic N_{CCN} - SS or AR - SS power-law fits to predict N_{CCN}, the prediction is better by using the real-time PNSD combined with the parameterized κ, including a constant κ of 0.3, the bulk κ_{chem}, and the κ - D_p power-law fit. However, assuming a constant κ of 0.3 recommended for continental aerosol (Andreae and Rosenfeld., 2008) or the bulk κ_{chem} calculated from aerosol chemical composition both cause significant overestimations of the N_{CCN} with approximately 10% in median for all SS conditions, which theoretically cause 3.2% overestimation of cloud optical thickness, amounting to

approximately one-third of the direct radiative forcing from a doubling CO_2 (Lee et al., 1997). And, the strength of the autoconversion process in cloud could be underestimated (Liu et al., 2006). ~~with about 30% in median, especially at *SS* = 0.1% in summer. Generally, the performances of the latter (the bulk κ_{chem}) are slightly better than the former (a constant κ of 0.3) on account of the lower uncertainty at each given season and *SS* condition.~~ Size-resolved κ improves the N_{CCN} prediction. We recommend applying the κ - D_p power-law fit for N_{CCN} prediction, which obtains the best prediction among the five schemes.

The κ - D_p power-law fit presented in this study could apply to other rural regions. However, it may cause considerable deviations for different aerosol background regions. For instance, using the κ - D_p power-law fit measured in urban Budapest (Salma et al., 2021) for predicting Melpitz N_{CCN}, it could cause a 39% underestimation of N_{CCN} in median for all *SS* conditions. Additionally, the seasonal difference of the κ - D_p relationship needs to be considered carefully for N_{CCN} prediction. At Melpitz, if the κ - D_p power-law fit measured in summer was used for predicting N_{CCN} in winter, it could cause a 13% underestimation of N_{CCN} in median for all *SS* conditions. Although the κ - D_p relationships are similar measured in rural stations, but when comparing the different urban stations (e.g., shanghai vs. Budapest in Figure 8), these relationships are clearly different and the reasons for the difference are still unclear. Thus, long-term monodisperse CCN measurements are still needed not only to obtain the κ - D_p relationships for different regions and for different seasons, but furtherly investigate the reasons for the difference of the κ - D_p relationships measured at same type of regions. Finally for the purpose of predicting N_{CCN}, the measurements of monodisperse CCN and particle chemical compositions are more expected, compared to the polydisperse

CCN measurements.

~~At Melpitz, using the real-time PNSD combined with the κ - D_p power-law fit could narrow down the uncertainty of N_{CCN} prediction within 10% in median for all SS conditions (0.1–0.7%) and seasons. The κ - D_p power-law fit presented in this study could apply to other rural and continental regions with similar aerosol background conditions. To our knowledge, the κ - D_p power-law fit is the first time applied to predict N_{CCN}. Additionally, the mean κ value over D_p of 100 to 200 nm also works well to predict N_{CCN} at a relatively low SS of less than 0.2%.~~

Appendix ~~B~~ Notation list

A	comprehensive parameter for $\sigma_{s/a}$, M_w, R, T, and ρ_w in equation (2b)
a	lower limit for calculating critical diameters at the set-nominal supersaturations in equation (1)
ACI	aerosol and cloud interactions
ACSM	aerosol chemical species monitor
ACTRIS	Aerosol, Clouds and Trace Gases Research Infrastructure
AF	activated fraction, i.e., N_{CCN}/N_{CN}
AIEs	aerosol indirect effects
AR	activation ratio, i.e., N_{CCN}/N_{aero}
b	upper limit for calculating critical diameters at the set-nominal supersaturations in equation (1)
BC	black carbon
CN	condensation nuclei
CCN	cloud condensation nuclei
CCNC	cloud condensation nuclei counter
$coef$	coefficient in κ - D_p power-law fit
CPC	condensation particle counter
D_p	diameter of the dry particle
D_c	critical diameter of the dry particle
D_X	D at which X % of the particles are activated
$(D_{75} - D_{25})/D_c$	degree of external mixture
D-MPSS	Dual-mobility particle size spectrometer
DMA	differential mobility analyzer
eBC	equivalent black carbon
f_{BC}	mass fraction of BC in submicron aerosol
$f_{nitrate}$	mass fraction of nitrate in submicron aerosol
f_{org}	mass fraction of organics in submicron aerosol
$f_{sulfate}$	mass fraction of sulfate in submicron aerosol
GMD	geometric mean diameter of PNSD
M_w	molecular weight of water
N_{aero}	number concentration of aerosol with a D_p ~~ranging~~ range of 10 to 800 nm
N_C	number concentration of cloud droplet
N_{CN}	number concentration of CN
N_{CCN}	number concentration of CCN
NPF	new particle formation
OA	organic aerosol
PM_{10}	particulate matter with the $D_p < 10$ µm
PNSD	particle number size distribution
R	universal gas constant
R^2	coefficient of determination
RD	relative deviation between the predicted N_{CCN} and the measured one
SI	Supporting information

SS	supersaturation
SOA	secondary organic aerosol
T	temperature
σ_s	represent the shape of the sigmoid function
$\sigma_{s/a}$	droplet surface tension
κ	hygroscopicity factor of aerosol particle
κ_i	κ *of* each component
κ_{CCN}	κ calculated from the monodisperse CCN measurements
κ_{chem}	κ calculated from the aerosol chemical measurements
ε_i	volume fraction of each component
ρ_w	density of the liquid water

Data availability.

The data used in this study are available from Silvia Henning (henning@tropos.de) upon request and https://doi.org/10.1594/PANGAEA.938215.

Author contributions.

AW, SH and LP designed the research. SH and LP collected the data at Melpitz. YW performed the data analysis and prepared the paper. All co-authors contributed to interpretation of the results as well as paper review and editing.

Competing interests.

The authors declare that they have no conflict of interest.

Acknowledgments.

This research has been supported by the H2020 research infrastructures (grant nos. ACTRIS (262254) and ACTRIS-2 (654109)), the European Cooperation in Science and Technology (grant no. COLOSSAL CA16109), the German Federal Environment Ministry (BMU) grants F&E 370343200 (German title: “Erfassung der Zahl feiner und ultrafeiner Partikel in der Außenluft”), 2008–2010, and F&E 371143232 (German title: “Trendanalysen gesundheitsgefährdender Fein- und Ultrafeinstaubfraktionen unter Nutzung der im German Ultrafine Aerosol Network (GUAN) ermittelten

Immissionsdaten durch Fortführung und Interpretation der Messreihen”), 2012–2014. This research has received funding from the Deutsche Forschungsgemeinschaft (*DFG*, German Research Foundation, HE 6770/2), the National Natural Science Foundation of China under grant numbers 42205072, 42075066, 42075063, 42175099, and 42005067. The China Scholarship Council (no.202008320513) is acknowledged for supporting Yuan Wang financially. We thank Achim Grüner and René Rabe for the careful maintenance of the measurements on site.

References

Albrecht, B. A.: Aerosols, cloud microphysics, and fractional cloudiness, Science, 245(4923), 1227–1230, https://doi.org/10.1126/ science.245.4923.1227, 1989.

Andreae, M. O. and Rosenfeld, D.: Aerosol-cloud-precipitation interactions. Part 1. The nature and sources of cloud-active particles, Earth-Sci. Rev., 89, 13–41, https://doi.org/10.1016/j.earscirev.2008.03.001, 2008.

Birmili, W., Stratmann, F., and Wiedensohler, A.: Design of a DMA-based size spectrometer for a large particle size range and stable operation, J. Aerosol Sci., 30, 549–553, https://doi.org/10.1016/S0021-8502(98)00047-0, 1999.

Birmili, W., Weinhold, K., Nordmann, S., Wiedensohler, A., Spindler, G., Müller, K., Herrmann, H., Gnauk, T., Pitz, M., Cyrys, J., Flentje, H., Nickel, C., Kuhlbusch, T. A. J., and Löschau, G.: Atmospheric aerosol measurements in the German Ultrafine Aerosol Network (GUAN): Part 1 – soot and particle number size distribution, Gefahrst. Reinh. Luft., 69, 137–145, 2009.

Burkart, J., Steiner, G., Reischl, G., and Hitzenberger, R.: Longterm study of cloud condensation nuclei (CCN) activation of the atmospheric aerosol in Vienna, Atmos. Environ., 45, 5751–5759, https://doi.org/10.1016/j.atmosenv.2011.07.022, 2011.

Che, H., Zhang, X., Zhang, L., Wang, Y., Shen, X., Ma, Q., Sun, J., Zhong, J.: Prediction of size-resolved number concentration of cloud condensation nuclei and long-term measurements of their activation characteristics, Sci. Rep., 7, 5819, https://doi.org/10.1038/s41598-017-05998-3, 2017.

Chen, G., Canonaco, F., Tobler, A., Aas, W., Alastuey, A., Allan, J., Atabakhsh, S., Aurela, M., Baltensperger, U., Bougiatioti, A., Brito, J. F. D., Ceburnis, D., Chazeau, B., Chebaicheb, H., Daellenbach, K. R., Ehn, M., Haddad, I. E., Eleftheriadis, K., Favez, O., Flentje, H., Font, A., Fossum, K., Freney, E., Gini, M., Green, D. C., Heikkinen, L., Herrmann, H., Kalogridis, A., Keernik, H., Lhotka, R., Lin, C., Lunder, C., Maasikmets, M., Manousakas, M. I., Marchand, N., Marin, C., Marmureanu, L., Mihalopoulos, N., Močnik, G., Nęcki, J., O'Dowd, C., Ovadnevaite, J., Peter, T., Petit, J., Pikridas, M., Platt, S.M., Pokorná, P., Poulain, L., Priestman, M., Riffault, V., Rinaldi, M., Różański, K., Schwarz, J., Sciare, J., Simon, L., Skiba, A., Slowik, J. G., Sosedova, Y., Stavroulas, I., Styszko, K., Teinemaa, E., Timonen, H., Tremper, A., Vasilescu, J., Via, M., Vodička, P., Wiedensohler, A., Zografou, O., Minguillón, M.C., Prévôt, A.S.H.: European aerosol phenomenology − 8: Harmonised source apportionment of organic aerosol using 22 Year-long ACSM/AMS datasets, Environ. Int., 166, 107325, 2002.

Clegg, S., Brimblecombe, P., and Wexler, A.: Thermodynamic model of the system H+ - NH4+ - SO42− - NO3− - H2O at tropospheric temperatures. J. Phys. Chem. A, 102, 2137-2154,1998.

Crenn, V., Sciare, J., Croteau, P. L., Verlhac, S., Fröhlich, R., Belis, C. A., Aas, W., Äijälä, M., Alastuey, A., Artiñano, B., Baisnée, D., Bonnaire, N., Bressi, M., Canagaratna, M., Canonaco, F., Carbone, C., Cavalli, F., Coz, E., Cubison, M. J., Esser-Gietl, J. K., Green, D. C., Gros, V., Heikkinen, L., Herrmann, H., Lunder, C., Minguillón, M. C., Močnik, G., O'Dowd, C. D.,

Ovadnevaite, J., Petit, J.-E., Petralia, E., Poulain, L., Priestman, M., Riffault, V., Ripoll, A., Sarda-Estève, R., Slowik, J. G., Setyan, A., Wiedensohler, A., Baltensperger, U., Prévôt, A. S. H., Jayne, J. T., and Favez, O.: ACTRIS ACSM intercomparison – Part 1: Reproducibility of concentration and fragment results from 13 individual Quadrupole Aerosol Chemical Speciation Monitors (Q-ACSM) and consistency with co-located instruments, Atmos. Meas. Tech., 8, 5063–5087, https://doi.org/10.5194/amt-8-5063-2015, 2015.

Crippa, M., Canonaco, F., Lanz, V. A., Äijälä, M., Allan, J. D., Carbone, S., Capes, G., Ceburnis, D., Dall'Osto, M., Day, D. A., DeCarlo, P. F., Ehn, M., Eriksson, A., Freney, E., Hildebrandt Ruiz, L., Hillamo, R., Jimenez, J. L., Junninen, H., Kiendler-Scharr, A., Kortelainen, A.-M., Kulmala, M., Laaksonen, A., Mensah, A. A., Mohr, C., Nemitz, E., O'Dowd, C., Ovadnevaite, J., Pandis, S. N., Petäjä, T., Poulain, L., Saarikoski, S., Sellegri, K., Swietlicki, E., Tiitta, P., Worsnop, D. R., Baltensperger, U., and Prévôt, A. S. H.: Organic aerosol components derived from 25 AMS data sets across Europe using a consistent ME-2 based source apportionment approach, Atmos. Chem. Phys., 14, 6159–6176, https://doi.org/10.5194/acp-14-6159-2014, 2014.

Croft, B., Lohmann, U., Martin, R. V., Stier, P., Wurzler, S., Feichter, J., Posselt, R., and Ferrachat, S.: Aerosol size-dependent below-cloud scavenging by rain and snow in the ECHAM5-HAM, Atmos. Chem. Phys., 9, 4653–4675, https://doi.org/10.5194/acp-9-4653-2009, 2009.

Deng, Z. Z., Zhao, C. S., Ma, N., Liu, P. F., Ran, L., Xu, W. Y., Chen, J., Liang, Z., Liang, S., Huang, M. Y., Ma, X. C., Zhang, Q., Quan, J. N., Yan, P., Henning, S., Mildenberger, K., Sommerhage, E., Schäfer, M., Stratmann, F., and Wiedensohler, A.: Size-resolved and bulk activation properties of aerosols in the North China Plain, Atmos. Chem. Phys., 11, 3835–3846, https://doi.org/10.5194/acp-11-3835-2011, 2011.

Deng, Z. Z., Zhao, C. S., Ma, N., Ran, L., Zhou, G. Q., Lu, D. R., and Zhou, X. J.: An examination of parameterizations for the CCN number concentration based on in situ measurements of aerosol activation properties in the North China Plain, Atmos. Chem. Phys., 13, 6227–6237, https://doi.org/10.5194/acp-13-6227-2013, 2013.

Dusek, U., Frank, G., Hildebrandt, L., Curtius, J., Schneider, J., Walter, S., Chand, D., Drewnick, F., Hings, S., Jung, D., Borrmann, S., and Andreae, M. O.: Size matters more than chemistry for cloud-nucleating ability of aerosol particles. Science, 312(5778): 1375-1378, DOI: 10.1126/science.1125261, 2006.

Dusek, U., Frank, G., Curtius, J., Drewnick, F., Schneider, J., Kürten, A., Rose, D., Andreae, M. O., Borrmann, S., Pöschl, U.: Enhanced organic mass fraction and decreased hygroscopicity of cloud condensation nuclei (CCN) during new particle formation events, Geophys. Res. Lett. 37 (3), doi: 10.1029/2009GL040930, 2010.

Eichler, H., Cheng, Y. F., Birmili, W., Nowak, A., Wiedensohler, A., Brüggemann, E., Gnauk, T., Herrmann, H., Althausen, D., Ansmann, A., Engelmann, R., Tesche, M., Wendisch, M., Zhang, Y. H., Hu, M., Liu, S., and Zeng, L. M.: Hygroscopic properties and extinction of aerosol particles at ambient relative humidity in South-Eastern China, Atmos. Environ., 42, 6321–6334,

https://doi.org/10.1016/j.atmosenv.2008.05.007, 2008.

Fan, J., Leung, L. R., Li, Z., Morrison, H., Chen, H., Zhou, Y., Qian, Y., and Wang, Y.: Aerosol impacts on clouds and precipitation in eastern China: Results from bin and bulk microphysics, J. Geophys. Res., 117, D00K36, https://doi.org/10.1029/2011JD016537, 2012.

Fan, J., Rosenfeld, D., Zhang, Y., Giangrande, S. E., Li, Z., Machado, L. A. T., Martin, S. T., Yang, Y., Wang, J., Artaxo, P., Barbosa, H. M. J., Braga, R. C., Comstock, J. M., Feng, Z., Gao, W., Gomes, H. B., Mei, F., Pöhlker, C., Pöhlker, M. L., Pöschl, U., and Souza, R. A. F.: Substantial convection and precipitation enhancements by ultrafine aerosol particles, Science, 359(6374), 411–418, DOI: 10.1126/science.aan8461, 2018.

~~Fierce, L., Riemer, N., and Bond, T. C.: Toward reduced representation of mixing state for simulating aerosol effects on climate, Bull. Am. Meteorol. Soc., 98(5), 971–980, https://doi.org/10.1175/BAMS-D-16-0028.1, 2016.~~

Fors, E. O., Swietlicki, E., Svenningsson, B., Kristensson, A., Frank, G. P., and Sporre, M.: Hygroscopic properties of the ambient aerosol in southern Sweden – a two year study, Atmos. Chem. Phys., 11, 8343–8361, https://doi.org/10.5194/acp-11-8343-2011, 2011.

Freney, E., Zhang, Y., Croteau, P., Amodeo, T., Williams, L., Truong, F., Petit, J.-E., Sciare, J., Sarda-Esteve, R., Bonnaire, N., Arumae, T., Aurela, M., Bougiatioti, A., Mihalopoulos, N., Coz, E., Artinano, B., Crenn, V., Elste, T., Heikkinen, L., Poulain, L., Wiedensohler, A., Herrmann, H., Priestman, M., Alastuey, A., Stavroulas, I., Tobler, A., Vasilescu, J., Zanca, N., Canagaratna, M., Carbone, C., Flentje, H., Green, D., Maasikmets, M., Marmureanu, L., Minguillon, M. C., Prevot, A. S. H., Gros, V., Jayne, J., and Favez, O.: The second ACTRIS inter-comparison (2016) for Aerosol Chemical Speciation Monitors (ACSM): Calibration protocols and instrument performance evaluations, Aerosol Sci. Tech., 53, 830–842, https://doi.org/10.1080/02786826.2019.1608901, 2019.

Gunthe, S. S., King, S. M., Rose, D., Chen, Q., Roldin, P., Farmer, D. K., Jimenez, J. L., Artaxo, P., Andreae, M. O., Martin, S. T., and Pöschl, U.: Cloud condensation nuclei in pristine tropical rainforest air of Amazonia: size–esolved measurements and modeling of atmospheric aerosol composition and CCN activity, Atmos. Chem. Phys., 9, 7551–7575, https://doi.org/10.5194/acp-9-7551-2009, 2009.

Gunthe, S. S., Rose, D., Su, H., Garland, R. M., Achtert, P., Nowak, A., Wiedensohler, A., Kuwata, M., Takegawa, N., Kondo, Y., Hu, M., Shao, M., Zhu, T., Andreae, M. O., and Pöschl, U.: Cloud condensation nuclei (CCN) from fresh and aged air pollution in the megacity region of Beijing, Atmos. Chem. Phys., 11, 11023–11039, https://doi.org/10.5194/acp-11-11023-2011, 2011.

Gysel, M., Crosier, J., Topping, D. O., Whitehead, J. D., Bower, K. N., Cubison, M. J., Williams, P. I., Flynn, M. J., McFiggans, G. B., and Coe, H.: Closure study between chemical composition and hygroscopic growth of aerosol particles during TORCH2, Atmos. Chem. Phys., 7, 6131–6144, doi:10.5194/acp-7-6131-2007, 2007.

Gysel, M. and Stratmann, F.: WP3 – NA3: In-situ chemical, physical and optical properties of aerosols, Deliverable D3.11: Standardized protocol for CCN measurements, Tech. rep., http://https://actris-ecac.eu/ccn-nc.html, 2013.

Henning, S., Dieckmann, K., Ignatius, K., Schäfer, M., Zedler, P., Harris, E., Sinha, B., van Pinxteren, D., Mertes, S., Birmili, W., Merkel, M., Wu, Z., Wiedensohler, A., Wex, H., Herrmann, H., and Stratmann, F.: Influence of cloud processing on CCN activation behaviour in the Thuringian Forest, Germany during HCCT-2010, Atmos. Chem. Phys., 14, 7859–7868, https://doi.org/10.5194/acp-14-7859-2014, 2014.

IPCC.: Climate Change 2021: The Physical Science Basis. Contribution of Working Group I to the Sixth Assessment Report of the Intergovernmental Panel on Climate Change, (p. 1796), Cambridge University Press. In Press, 2021.

Jayachandran, V. N., Varghese, M., Murugavel, P., Todekar, K. S., Bankar, S. P., Malap, N., Dinesh, G., Safai, P. D., Rao, J., Konwar, M., Dixit, S., and Prabha, T. V.: Cloud condensation nuclei characteristics during the Indian summer monsoon over a rain-shadow region, Atmos. Chem. Phys., 20, 7307–7334, https://doi.org/10.5194/acp-20-7307-2020, 2020.

Jia, H., Ma, X., Yu, F., Liu, Y., Yin, Y.: Distinct impacts of increased aerosols on cloud droplet number concentration of stratus/stratocumulus and cumulus. Geophys. Res. Lett., 46(22): 13517–13525, https://doi.org/10.1029/2019GL085081, 2019.

Jurányi, Z., Tritscher, T., Gysel, M., Laborde, M., Gomes, L., Roberts, G., Baltensperger, U., and Weingartner, E.: Hygroscopic mixing state of urban aerosol derived from size-resolved cloud condensation nuclei measurements during the MEGAPOLI campaign in Paris, Atmos. Chem. Phys., 13, 6431–6446, https://doi.org/10.5194/acp-13-6431-2013, 2013.

Khain, P. A.: Notes on state-of-the-art investigations of aerosol effects on precipitation: A critical review, Environ. Res. Lett., 4(1), 015004, DOI: 10.1088/1748-9326/4/1/015004, 2009.

Kim, J. H., Yum, S. S., Shim, S., Kim, W. J., Park, M., Kim, J.-H., Kim, M.-H., and Yoon, S.-C.: On the submicron aerosol distributions and CCN number concentrations in and around the Korean Peninsula, Atmos. Chem. Phys., 14, 8763–8779, https://doi.org/10.5194/acp-14-8763-2014, 2014.

Köhler, H.: The nucleus in and the growth of hygroscopic droplets, Trans Farad Soc, 32, 1152–1161, https://doi.org/10.1039/TF9363201152, 1936.

Kristensen, T. B., Müller, T., Kandler, K., Benker, N., Hartmann, M., Prospero, J. M., Wiedensohler, A., and Stratmann, F.: Properties of cloud condensation nuclei (CCN) in the trade wind marine boundary layer of the western North Atlantic, Atmos. Chem. Phys., 16, 2675–2688, https://doi.org/10.5194/acp-16-2675-2016, 2016.

Kuang, Y., He, Y., Xu, W., Zhao, P., Cheng, Y., Zhao, G., Tao, J., Ma, N., Su, H., Zhang, Y., Sun, J., Cheng, P., Yang, W., Zhang, S., Wu, C., Sun, Y., and Zhao, C.: Distinct diurnal variation in organic aerosol hygroscopicity and its relationship with oxygenated organic aerosol, Atmos. Chem. Phys., 20, 865–880, https://doi.org/10.5194/acp-20-865-2020, 2020.

Kulmala, M., Petäjä, T., Nieminen, T., Sipilä, M., Manninen, H. E., Lehtipalo, K., Dal Maso, M., Aalto, P. P., Junninen, H., Paasonen, P., Riipinen, I., Lehtinen, K. E. J., Laaksonen, A., and Kerminen, V.-M.: Measurement of the nucleation of atmospheric aerosol particles, Nat. Protocols, 7, 1651–1667, https://doi.org/10.1038/nprot.2012.091, 2012.

Lee, W., Iacobellis, S. F., and Somerville, R. C. J.: Cloud Radiation Forcings and Feedbacks: General Circulation Model Tests and Observational Validation, Journal of Climate, 10(10), 2479-2496, 1997.

Liu, Y., Daum, P. H., McGraw, R., and Miller, M.: Generalized threshold function accounting for effect of relative dispersion on threshold behavior of autoconversion process, Geophys. Res. Lett., 33(11), L11804, 2006.

Liu, J. and Li, Z.: Estimation of cloud condensation nuclei concentration from aerosol optical quantities: influential factors and uncertainties, Atmos. Chem. Phys., 14, 471–483, https://doi.org/10.5194/acp-14-471-2014, 2014.

Ma, N. and Birmili, W.: Estimating the contribution of photochemical particle formation to ultrafine particle number averages in an urban atmosphere, Sci. Total Environ., 512/513, 154–166, https://doi.org/10.1016/j.scitotenv.2015.01.009, 2015

Massling, A., Stock, M., Wehner, B., Wu, Z. J., Hu, M., Brueggemann, E., Gnauk, T., Herrmann, H., and Wiedensohler, A.: Size segregated water uptake of the urban submicrometer aerosol in Beijing, Atmos. Environ., 43, 1578–1589, https://doi.org/10.1016/j.atmosenv.2008.06.003, 2009.

Mazoyer, M., Burnet, F., Denjean, C., Roberts, G. C., Haeffelin, M., Dupont, J.-C., and Elias, T.: Experimental study of the aerosol impact on fog microphysics, Atmos. Chem. Phys., 19, 4323–4344, https://doi.org/10.5194/acp-19-4323-2019, 2019.

~~McFiggans, G., Artaxo, P., Baltensperger, U., Coe, H., Facchini, M. C., Feingold, G., Fuzzi, S., Gysel, M., Laaksonen, A., Lohmann, U., Mentel, T. F., Murphy, D. M., O'Dowd, C.D., Snider, J. R., and Weingartner, E.: The effect of physical and chemical aerosol properties on warm cloud droplet activation, Atmos. Chem. Phys., 6, 2593-2649, https://doi.org/10.5194/acp-6-2593-2006, 2006.~~

Müller, T., Henzing, J. S., de Leeuw, G., Wiedensohler, A., Alastuey, A., Angelov, H., Bizjak, M., Collaud Coen, M., Engström, J. E., Gruening, C., Hillamo, R., Hoffer, A., Imre, K., Ivanow, P., Jennings, G., Sun, J. Y., Kalivitis, N., Karlsson, H., Komppula, M., Laj, P., Li, S.-M., Lunder, C., Marinoni, A., Martins dos Santos, S., Moerman, M., Nowak, A., Ogren, J. A., Petzold, A., Pichon, J. M., Rodriquez, S., Sharma, S., Sheridan, P. J., Teinilä, K., Tuch, T., Viana, M., Virkkula, A., Weingartner, E., Wilhelm, R., and Wang, Y. Q.: Characterization and intercomparison of aerosol absorption photometers: result of two intercomparison workshops, Atmos. Meas. Tech., 4, 245–268, https://doi.org/10.5194/amt-4-245-2011, 2011

Nenes, A., Charlson, R. J., Facchini, M. C., Kulmalam M., Laaksonen, A., and Seinfeld, J. H.: Can chemical effects on cloud droplet number rival the first indirect effect? Geophys. Res. Lett.,

29(17): 29-1-29-4, doi:10.1029/2002GL015295, 2002.

Ng, N. L., Herndon, S. C., Trimborn, A., Canagaratna, M. R., Croteau, P. L., Onasch, T. B., Sueper, D., Worsnop, D. R., Zhang, Q., Sun, Y. L., and Jayne, J. T.: An Aerosol Chemical Speciation Monitor (ACSM) for Routine Monitoring of the Composition and Mass Concentrations of Ambient Aerosol, Aerosol Sci. Tech., 45, 780–794, https://doi.org/10.1080/02786826.2011.560211, 2011.

Ovadnevaite, J., Zuend, A., Laaksonen, A., Sanchez, K. J., Roberts, G., Ceburnis, D., Decesari, S., Rinaldi, M., Hodas, N., Facchini, M. C., Seinfeld, J. H. and O' Dowd, C.: Surface tension prevails over solute effect in organic-influenced cloud droplet activation, Nature, 546(7660), 637–641, doi:10.1038/nature22806, 2017.

Paramonov, M., Kerminen, V.-M., Gysel, M., Aalto, P. P., Andreae, M. O., Asmi, E., Baltensperger, U., Bougiatioti, A., Brus, D., Frank, G. P., Good, N., Gunthe, S. S., Hao, L., Irwin, M., Jaatinen, A., Jurányi, Z., King, S. M., Kortelainen, A., Kristensson, A., Lihavainen, H., Kulmala, M., Lohmann, U., Martin, S. T., McFiggans, G., Mihalopoulos, N., Nenes, A., O'Dowd, C. D., Ovadnevaite, J., Petäjä, T., Pöschl, U., Roberts, G. C., Rose, D., Svenningsson, B., Swietlicki, E., Weingartner, E., Whitehead, J., Wiedensohler, A., Wittbom, C., and Sierau, B.: A synthesis of cloud condensation nuclei counter (CCNC) measurements within the EUCAARI network, Atmos. Chem. Phys., 15, 12211–12229, https://doi.org/10.5194/acp-15-12211-2015, 2015.

Petters, M. D., and Kreidenweis, S. M.: A single parameter representation of hygroscopic growth and cloud condensation nuclei activity, Atmos. Chem. Phys., 7, 1961-1971, https://doi.org/10.5194/acp-7-1961-2007, 2007.

Petzold, A. and Schönlinner, M.: Multi-angle absorption photometry - a new method for the measurement of aerosol light absorption and atmospheric black carbon, J. Aerosol Sci., 35, 421–441, https://doi.org/10.1016/j.jaerosci.2003.09.005, 2004.

Poulain, L., Wu, Z., Petters, M. D., Wex, H., Hallbauer, E., Wehner, B., Massling, A., Kreidenweis, S. M., and Stratmann, F.: Towards closing the gap between hygroscopic growth and CCN activation for secondary organic aerosols – Part 3: Influence of the chemical composition on the hygroscopic properties and volatile fractions of aerosols, Atmos. Chem. Phys., 10, 3775–3785, https://doi.org/10.5194/acp-10-3775-2010, 2010.

Poulain, L., Spindler, G., Birmili, W., Plass-Dülmer, C., Wiedensohler, A., and Herrmann, H.: Seasonal and diurnal variations of particulate nitrate and organic matter at the IfT research station Melpitz, Atmos. Chem. Phys., 11, 12579–12599, https://doi.org/10.5194/acp-11-12579-2011, 2011.

Poulain, L., Birmili, W., Canonaco, F., Crippa, M., Wu, Z. J., Nordmann, S., Spindler, G., Prévôt, A. S. H., Wiedensohler, A., and Herrmann, H.: Chemical mass balance of 300 °C non-volatile particles at the tropospheric research site Melpitz, Germany, Atmos. Chem. Phys., 14, 10145–10162, https://doi.org/10.5194/acp-14-10145-2014, 2014.

Poulain, L., Spindler, G., Grüner, A., Tuch, T., Stieger, B., van Pinxteren, D., Petit, J.-E., Favez, O.,

Herrmann, H., and Wiedensohler, A.: Multi-year ACSM measurements at the central European research station Melpitz (Germany) – Part 1: Instrument robustness, quality assurance, and impact of upper size cutoff diameter, Atmos. Meas. Tech., 13, 4973–4994, https://doi.org/10.5194/amt-13-4973-2020, 2020.

Pöhlker, M. L., Pöhlker, C., Ditas, F., Klimach, T., Hrabe de Angelis, I., Araújo, A., Brito, J., Carbone, S., Cheng, Y., Chi, X., Ditz, R., Gunthe, S. S., Kesselmeier, J., Könemann, T., Lavrič, J. V., Martin, S. T., Mikhailov, E., Moran-Zuloaga, D., Rose, D., Saturno, J., Su, H., Thalman, R., Walter, D., Wang, J., Wolff, S., Barbosa, H. M. J., Artaxo, P., Andreae, M. O., and Pöschl, U.: Long-term observations of cloud condensation nuclei in the Amazon rain forest – Part 1: Aerosol size distribution, hygroscopicity, and new model parametrizations for CCN prediction, Atmos. Chem. Phys., 16, 15709–15740, https://doi.org/10.5194/acp-16-15709-2016, 2016.

Pöhlker, M. L., Ditas, F., Saturno, J., Klimach, T., Hrabě de Angelis, I., Araùjo, A. C., Brito, J., Carbone, S., Cheng, Y., Chi, X., Ditz, R., Gunthe, S. S., Holanda, B. A., Kandler, K., Kesselmeier, J., Könemann, T., Krüger, O. O., Lavrič, J. V., Martin, S. T., Mikhailov, E., Moran-Zuloaga, D., Rizzo, L. V., Rose, D., Su, H., Thalman, R., Walter, D., Wang, J., Wolff, S., Barbosa, H. M. J., Artaxo, P., Andreae, M. O., Pöschl, U., and Pöhlker, C.: Long-term observations of cloud condensation nuclei over the Amazon rain forest – Part 2: Variability and characteristics of biomass burning, long-range transport, and pristine rain forest aerosols, Atmos. Chem. Phys., 18, 10289–10331, https://doi.org/10.5194/acp-18-10289-2018, 2018.

Ramanathan, V., Crutzen, P. J., Kiehl, J. T., and Rosenfeld, D.: Aerosols, climate, and the hydrological cycle, Science, 294(5549), 2119–2124. https://doi.org/10.1126/science.1064034, 2001.

Rastak, N., Pajunoja, A., Acosta Navarro, J. C., Ma, J., Song, M., Partridge, D. G., Kirkevåg, A., Leong, Y., Hu, W. W., Taylor, N. F., Lambe, A., Cerully, K., Bougiatioti, A., Liu, P., Krejci, R., Petäjä, T., Percival, C., Davidovits, P., Worsnop, D. R., Ekman, A. M. L., Nenes, A., Martin, S., Jimenez, J. L., Collins, D. R., Topping, D. O., Bertram, A. K., Zuend, A., Virtanen, A., and Riipinen, I.: Microphysical explanation of the RH-dependent water affinity of biogenic organic aerosol and its importance for climate, Geophys. Res. Lett., 44, 5167–5177, https://doi.org/10.1002/2017gl073056, 2017.

Roberts, G. C., and Nenes, A.: A continuous-flow streamwise thermal-gradient CCN chamber for atmospheric measurements, Aerosol Sci. Tech., 39(3), 206–221, https://doi.org/10.1080/027868290913988, 2005.

Rose, D., Gunthe, S. S., Mikhailov, E., Frank, G. P., Dusek, U., Andreae, M. O., and Pöschl, U.: Calibration and measurement uncertainties of a continuous-flow cloud condensation nuclei counter (DMT-CCNC): CCN activation of ammonium sulfate and sodium chloride aerosol particles in theory and experiment, Atmos. Chem. Phys., 8, 1153–1179, https://doi.org/10.5194/acp-8-1153-2008, 2008.

Rose, D., Nowak, A., Achtert, P., Wiedensohler, A., Hu, M., Shao, M., Zhang, Y., Andreae, M. O.,

and Pöschl, U.: Cloud condensation nuclei in polluted air and biomass burning smoke near the mega-city Guangzhou, China – Part 1: Size-resolved measurements and implications for the modeling of aerosol particle hygroscopicity and CCN activity, Atmos. Chem. Phys., 10, 3365–3383, https://doi.org/10.5194/acp-10-3365-2010, 2010.

Rose, D., Gunthe, S. S., Su, H., Garland, R. M., Yang, H., Berghof, M., Cheng, Y. F., Wehner, B., Achtert, P., Nowak, A., Wiedensohler, A., Takegawa, N., Kondo, Y., Hu, M., Zhang, Y., Andreae, M. O., and Pöschl, U.: Cloud condensation nuclei in polluted air and biomass burning smoke near the megacity Guangzhou, China – Part 2: Size-resolved aerosol chemical composition, diurnal cycles, and externally mixed weakly CCN-active soot particles, Atmos. Chem. Phys., 11, 2817–2836, https://doi.org/10.5194/acp-11-2817-2011, 2011

Rosenfeld, D., Zhu, Y., Wang, M., Zheng, Y., Goren, T., and Yu, S.: Aerosol-driven droplet concentrations dominate coverage and water of oceanic low-level clouds, science, 363(6427), DOI: 10.1126/science.aav0566, 2019.

Salma, I., Thén, W., Vörösmarty, M., and Gyöngyösi, A. Z.: Cloud activation properties of aerosol particles in a continental Central European urban environment, Atmos. Chem. Phys., 21, 11289–11302, https://doi.org/10.5194/acp-21-11289-2021, 2021.

~~Salma, I., Thén, W., Vörösmarty, M., and Gyöngyösi, A. Z.: Cloud droplet activation in a continental Central European urban environment, Atmos. Chem. Phys. Discuss., https://doi.org/10.5194/acp-2021-305, in review, 2021.~~

Schmale, J., Henning, S., Decesari, S., Henzing, B., Keskinen, H., Sellegri, K., Ovadnevaite, J., Pöhlker, M. L., Brito, J., Bougiatioti, A., Kristensson, A., Kalivitis, N., Stavroulas, I., Carbone, S., Jefferson, A., Park, M., Schlag, P., Iwamoto, Y., Aalto, P., Äijälä, M., Bukowiecki, N., Ehn, M., Frank, G., Fröhlich, R., Frumau, A., Herrmann, E., Herrmann, H., Holzinger, R., Kos, G., Kulmala, M., Mihalopoulos, N., Nenes, A., O'Dowd, C., Petäjä, T., Picard, D., Pöhlker, C., Pöschl, U., Poulain, L., Prévôt, A. S. H., Swietlicki, E., Andreae, M. O., Artaxo, P., Wiedensohler, A., Ogren, J., Matsuki, A., Yum, S. S., Stratmann, F., Baltensperger, U., and Gysel, M.: Long-term cloud condensation nuclei number concentration, particle number size distribution and chemical composition measurements at regionally representative observatories, Atmos. Chem. Phys., 18, 2853–2881, https://doi.org/10.5194/acp-18-2853-2018, 2018.

Seinfeld, J. H., and Pandis, S. N.: Atmospheric chemistry and physics: From air pollution to climate change, Hoboken: John Wiley and Sons, 2016.

Sihto, S.-L., Mikkilä, J., Vanhanen, J., Ehn, M., Liao, L., Lehtipalo, K., Aalto, P. P., Duplissy, J., Petäjä, T., Kerminen, V.-M., Boy, M., and Kulmala, M.: Seasonal variation of CCN concentrations and aerosol activation properties in boreal forest, Atmos. Chem. Phys., 11, 13269–13285, https://doi.org/10.5194/acp-11-13269-2011, 2011.

Singla, V., Mukherjee, S., Safai, P. D., Meena, G. S., Dani, K. K., Pandithurai, G.: Role of organic aerosols in CCN activation and closure over a rural background site in Western Ghats, India, Atmos. Environ., 158, 148-159, https://doi.org/10.1016/j.atmosenv.2017.03.037, 2017.

Stokes, R. H. and Robinson, R. A.: Interactions in Aqueous Nonelectrolyte Solutions. I. Solute-Solvent Equilibria, J. Phys. Chem., 70, 2126–2130, DOI: 10.1021/j100879a010, 1966.

Su, H., Rose, D., Cheng, Y. F., Gunthe, S. S., Massling, A., Stock, M., Wiedensohler, A., Andreae, M. O., and Pöschl, U.: Hygroscopicity distribution concept for measurement data analysis and modeling of aerosol particle mixing state with regard to hygroscopic growth and CCN activation, Atmos. Chem. Phys., 10, 7489–7503, https://doi.org/10.5194/acp-10-7489-2010, 2010.

Twomey, S.: The nuclei of natural cloud formation part II: The supersaturation in natural clouds and the variation of cloud droplet concentration, Geofisica Pura e Applicata, 43, 243–249, DOI: 10.1007/BF01993560, 1959.

Twomey, S.: Pollution and the planetary albedo, Atmos. Environ., 8(12), 1251–1256, https://doi.org/10.1016/0004-6981(74)90004-3, 1974.

Twomey, S.: The influence of pollution on the shortwave albedo of clouds, J. Atmos. Sci., 34(7), 1149–1152, https://doi.org/10.1175/1520-0469(1977)034<1149:TIOPOT>2.0.CO;2, 1977.

~~Tuch, T. M., Haudek, A., Müller, T., Nowak, A., Wex, H., and Wiedensohler, A.: Design and performance of an automatic regenerating adsorption aerosol dryer for continuous operation at monitoring sites, Atmos. Meas. Tech., 2, 417–422, https://doi.org/10.5194/amt-2-417-2009, 2009.~~

van Pinxteren, D., Fomba, K. W., Spindler, G., Müller, K., Poulain, L., Iinuma, Y., Loschau, G., Hausmann, A., and Herrmann, H.: Regional air quality in Leipzig, Germany: detailed source apportionment of size-resolved aerosol particles and compar ison with the year 2000, Faraday Discuss., 189, 291–315, https://doi.org/10.1039/c5fd00228a, 2016.

Varghese, M., Prabha, T. V., Malap, N., Resmi, E. A., Murugavel, P., Safai, P. D., Axisa, D., Pandithurai, G., and Dani, K.: Airborne and ground based CCN spectral characteristics: Inferences from CAIPEEX–2011, Atmos. Environ., 125, 324–336, https://doi.org/10.1016/j.atmosenv.2015.06.041, 2016.

Vepsäläinen, S., Calderón, S. M., Malila, J., and Prisle, N. L.: Comparison of six approaches to predicting droplet activation of surface active aerosol – Part 1: moderately surface active organics, Atmos. Chem. Phys., 22, 2669–2687, https://doi.org/10.5194/acp-22-2669-2022, 2022.

Wang, Y., Wan, Q., Meng, W., Liao, F., Tan, H., and Zhang, R.: Long-term impacts of aerosols on precipitation and lightning over the Pearl River Delta megacity area in China, Atmos. Chem. Phys., 11, 12421–12436, https://doi.org/10.5194/acp-11-12421-2011, 2011.

Wang, Y., Li, Z., Zhang, Y., Du, W., Zhang, F., Tan, H., Xu, H., Fan, T., Jin, X., Fan, X., Dong, Z., Wang, Q., and Sun, Y.: Characterization of aerosol hygroscopicity, mixing state, and CCN activity at a suburban site in the central North China Plain, Atmos. Chem. Phys., 18, 11739–11752, https://doi.org/10.5194/acp-18-11739-2018, 2018a.

Wang, Y., Wu, Z., Ma, N., Wu, Y., Zeng, L., Zhao, C., and Wiedensohler, A.: Statistical analysis and

parameterization of the hygroscopic growth of the sub-micrometer urban background aerosol in Beijing, Atmos. Environ., 175, 184–191, https://doi.org/10.1016/j.atmosenv.2017.12.003, 2018b.

Wang, Y., Niu, S., Lv, J., Lu, C., Xu, X., Wang, Y., Ding, J., Zhang, H., Wang, T., and Kang, B.: A new method for distinguishing unactivated particles in cloud condensation nuclei measurements: Implications for aerosol indirect effect evaluation, Geophys. Res. Lett., 46, 14,185–14,194, https://doi.org/10.1029/2019GL085379, 2019.

Wang, Z., Birmili, W., Hamed, A., Wehner, B., Spindler, G., Pei, X., Wu, Z., Cheng, Y., Su, H., and Wiedensohler, A.: Contributions of volatile and nonvolatile compounds (at 300°C) to condensational growth of atmospheric nanoparticles: An assessment based on 8.5 years of observations at the Central Europe background site Melpitz, J. Geophys. Res. Atmos., 122, 485–497, doi:10.1002/2016JD025581, 2017.

Wiedensohler, A.: An approximation of the bipolar charge distribution for particles in the sub-micron size range, J. Aerosol Sci., 19, 387–389, DOI: 10.1016/0021-8502(88)90278-9, 1988.

Wiedensohler, A., Birmili, W., Nowak, A., Sonntag, A., Weinhold, K., Merkel, M., Wehner, B., Tuch, T., Pfeifer, S., Fiebig, M., Fjäraa, A. M., Asmi, E., Sellegri, K., Depuy, R., Venzac, H., Villani, P., Laj, P., Aalto, P., Ogren, J. A., Swietlicki, E., Williams, P., Roldin, P., Quincey, P., Hüglin, C., Fierz-Schmidhauser, R., Gysel, M., Weingartner, E., Riccobono, F., Santos, S., Grüning, C., Faloon, K., Beddows, D., Harrison, R., Monahan, C., Jennings, S. G., O'Dowd, C. D., Marinoni, A., Horn, H.-G., Keck, L., Jiang, J., Scheckman, J., McMurry, P. H., Deng, Z., Zhao, C. S., Moerman, M., Henzing, B., de Leeuw, G., Löschau, G., and Bastian, S.: Mobility particle size spectrometers: harmonization of technical standards and data structure to facilitate high quality long-term observations of atmospheric particle number size distributions, Atmos. Meas. Tech., 5, 657–685, https://doi.org/10.5194/amt-5-657-2012, 2012.

Wiedensohler, A., Wiesner, A., Weinhold, K., Birmili, W., Hermann, M., Merkel, M., Muller, T., Pfeifer, S., Schmidt, A., Tuch, T., Velarde, F., Quincey, P., Seeger, S., and Nowak, A.: Mobility particle size spectrometers: Calibration procedures and measurement uncertainties, Aerosol Sci. Tech., 52, 146–164, https://doi.org/10.1080/02786826.2017.1387229, 2018.

Wu, Z. J., Poulain, L., Birmili, W., Größ, J., Niedermeier, N., Wang, Z. B., Herrmann, H., and Wiedensohler, A.: Some insights into the condensing vapors driving new particle growth to CCN sizes on the basis of hygroscopicity measurements, Atmos. Chem. Phys., 15, 13071–13083, https://doi.org/10.5194/acp-15-13071-2015, 2015.

Wu, Z. J., Zheng, J., Shang, D. J., Du, Z. F., Wu, Y. S., Zeng, L. M., Wiedensohler, A., and Hu, M.: Particle hygroscopicity and its link to chemical composition in the urban atmosphere of Beijing, China, during summertime, Atmos. Chem. Phys., 16, 1123–1138, https://doi.org/10.5194/acp-16-1123-2016, 2016.

Ye, X., Tang, C., Yin, Z., Chen, J., Ma, Z., Kong, L., Yang, X., Gao, W., and Geng, F.: Hygroscopic growth of urban aerosol particles during the 2009 Mirage-Shanghai Campaign, Atmos.

Environ., 64, 263–269, https://doi.org/10.1016/j.atmosenv.2012.09.064, 2013.

Zdanovskii, B.: Novyi Metod Rascheta Rastvorimostei Elektrolitovv Mnogokomponentnykh Sistema, Zh. Fiz. Khim+, 22, 1478–1485, 1486–1495, 1948.

Zhang, F., Li, Y., Li, Z., Sun, L., Li, R., Zhao, C., Wang, P., Sun, Y., Liu, X., Li, J., Li, P., Ren, G., and Fan, T.: Aerosol hygroscopicity and cloud condensation nuclei activity during the AC3Exp campaign: implications for cloud condensation nuclei parameterization, Atmos. Chem. Phys., 14, 13423–13437, https://doi.org/10.5194/acp-14-13423-2014, 2014.

Zhang, F., Li, Z., Li, Y., Sun, Y., Wang, Z., Li, P., Sun, L., Wang, P., Cribb, M., Zhao, C., Fan, T., Yang, X., and Wang, Q.: Impacts of organic aerosols and its oxidation level on CCN activity from measurement at a suburban site in China, Atmos. Chem. Phys., 16, 5413–5425, https://doi.org/10.5194/acp-16-5413-2016, 2016.

Zhang, F., Wang, Y., Peng, J., Ren, J., Collins, D., Zhang, R., Sun, Y., Yang, X., and Li, Z.: Uncertainty in predicting CCN activity of aged and primary aerosols, J. Geophys. Res. Atmos., 122(21): 11,723-11,736, https://doi.org/10.1002/2017JD027058, 2017.

Zhao, C., Klein, S. A., Xie, S., Liu, X., Boyle, J. S., and Zhang, Y.: Aerosol first indirect effects on non-precipitating low-level liquid cloud properties as simulated by CAM5 at ARM sites, Geophys. Res. Lett., 39, L08806, https://doi.org/10.1029/2012GL051213, 2012.

Zhao, C., and Garrett, T. J.: Effects of Arctic haze on surface cloud radiative forcing, Geophys. Res. Lett., 42(2), 557–564, https://dx.doi.org/10.1002/2014GL062015, 2015

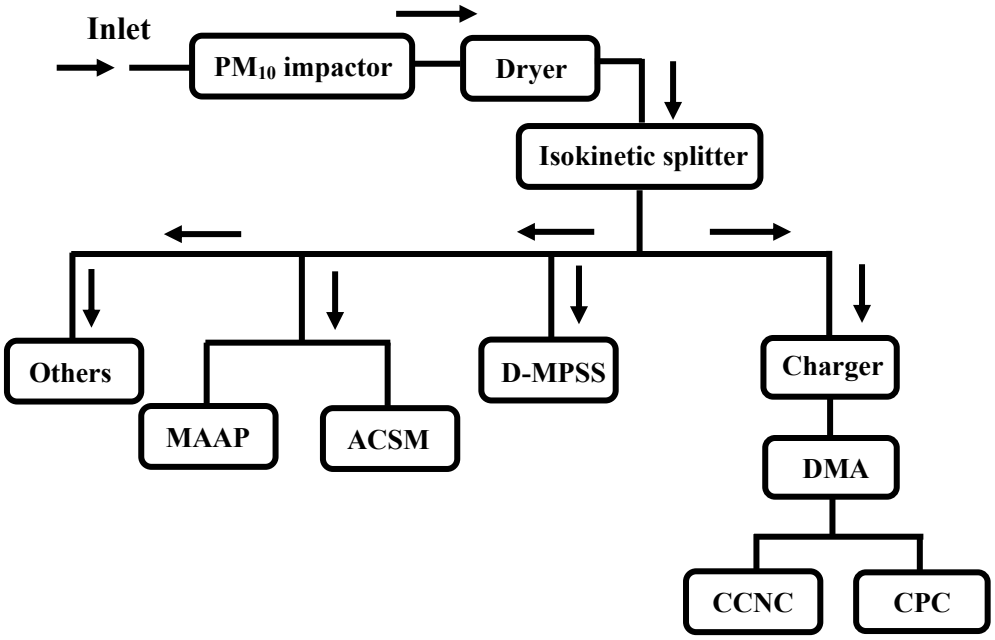

Figure 1. Schematic diagram of the experimental setup. D-MPSS — Dual-mobility particle size spectrometer, ACSM — aerosol chemical species monitor, MAAP — multi-angle absorption photometer, DMA — differential mobility analyzer, CPC — condensation particle counter, CCNC — cloud condensation nuclei counter.

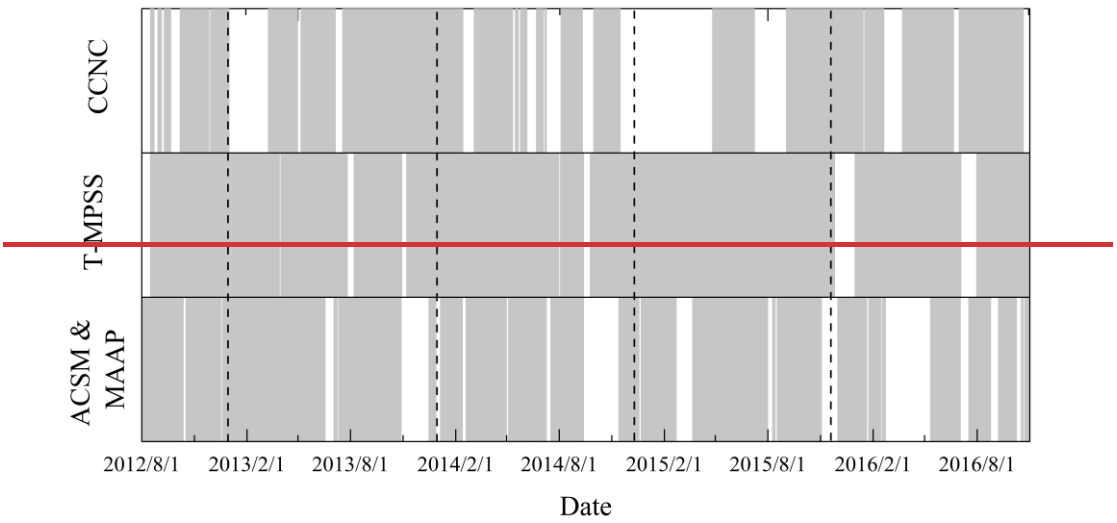

~~Figure 2. Coverage of the effective data represented by the gray columns.~~

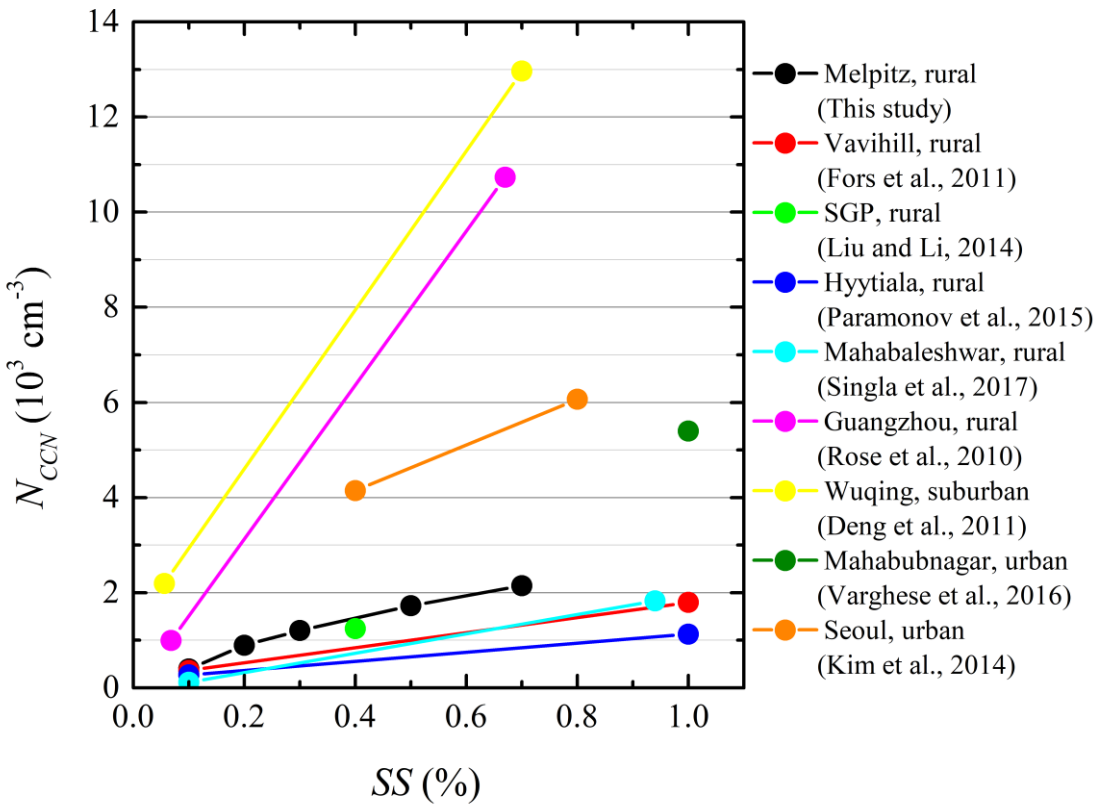

Figure 2. Relationship between CCN number concentration (N_{CCN}) and supersaturation (SS) measured at Melpitz and other stations.

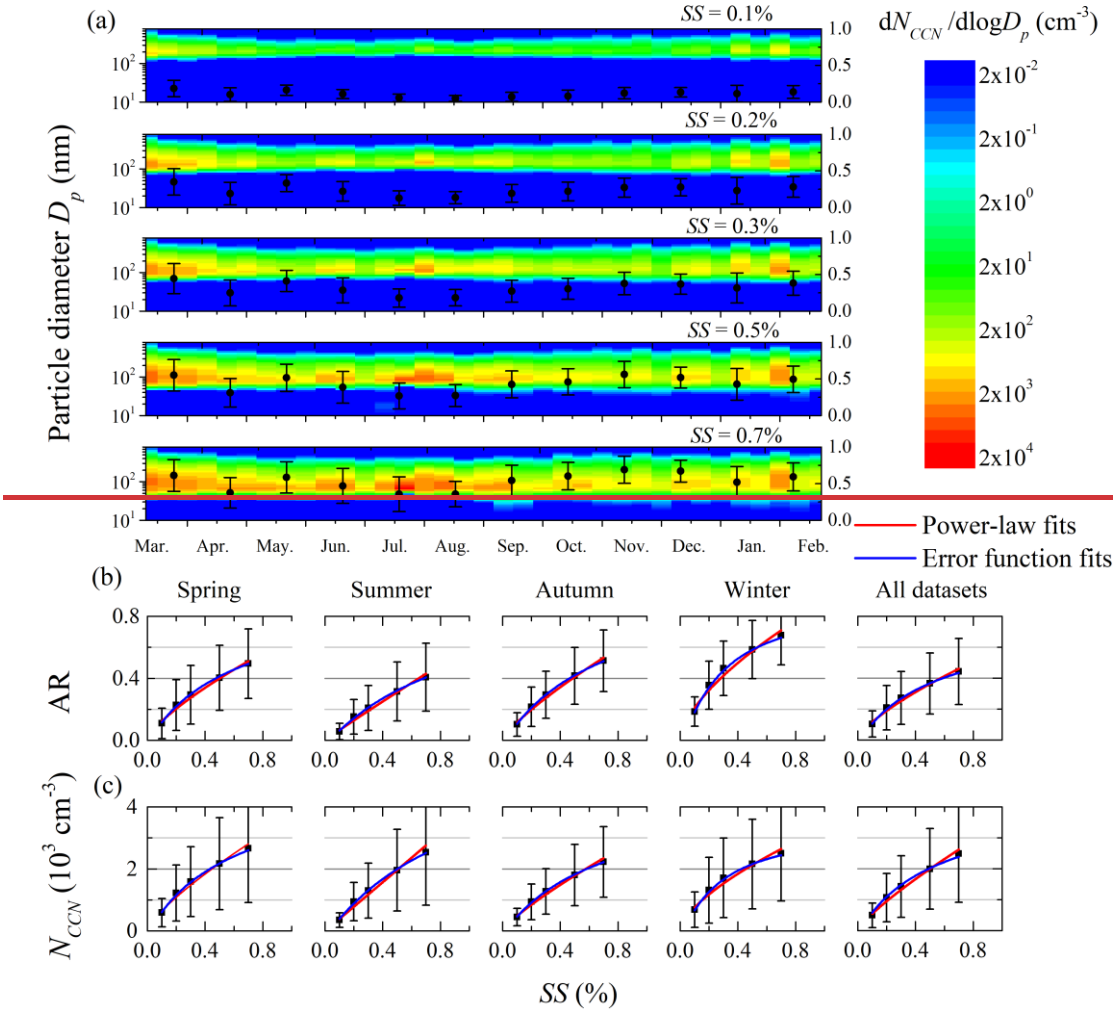

~~Figure 3. Seasonal variations of (a) CCN number size distributions and activation ratios (AR) at five different supersaturation (*SS*) conditions, (b) relationship between AR and *SS* for different seasons, and (c) relationship between CCN number concentration (N_{CCN}) and *SS* for different seasons. Error bar means one standard deviation. Red lines and blue lines are the fittings for AR vs. *SS* and N_{CCN} vs. *SS* with using the power-law function and the error function, respectively. Fitting results are shown in Table 3.~~

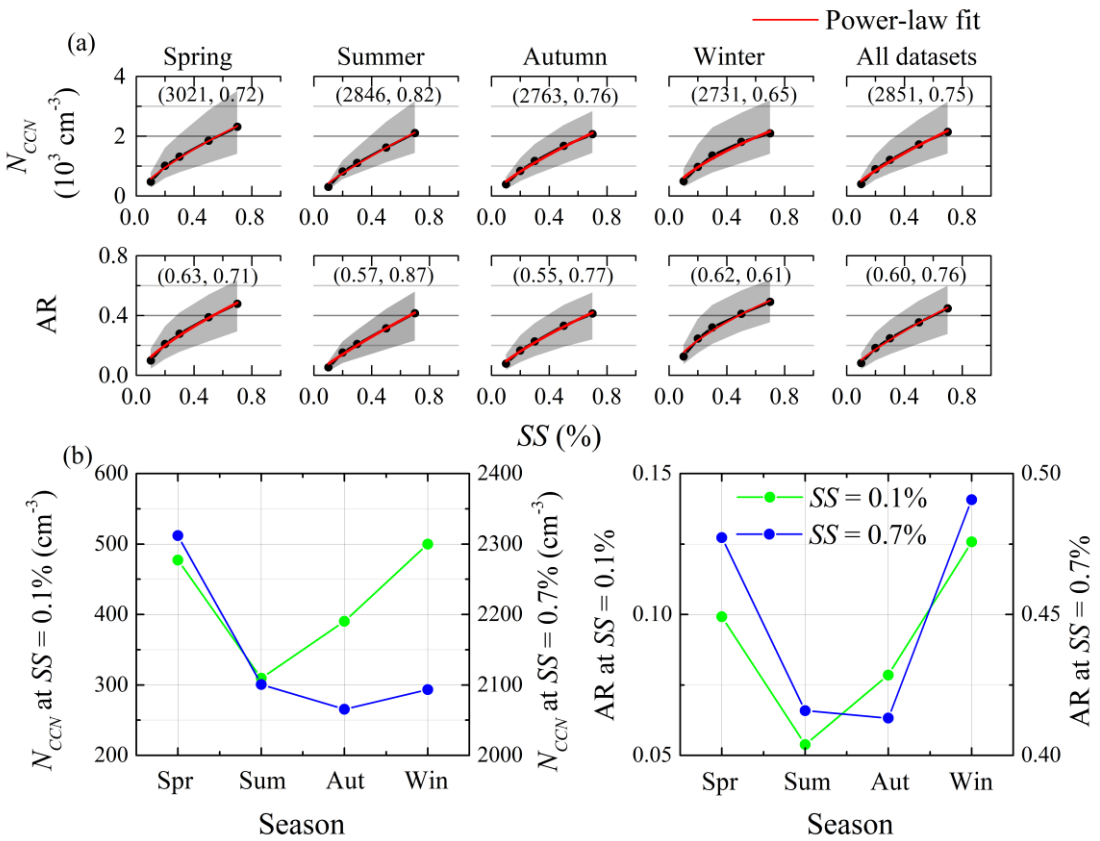

Figure 3. (a) Relationships between CCN number concentration (N_{CCN}) and supersaturation (SS), and relationship between activation ratios (AR) and SS for different seasons. (b) Seasonal trends of N_{CCN} and AR at SS = 0.1% and 0.7%. Dots represent the median values of N_{CCN} and AR. Shaded areas represent the values in the range from 25th to 75th percent. Red lines are power-law fittings for N_{CCN} (and AR) vs. SS. Two parameters of the fitting results are shown in brackets.

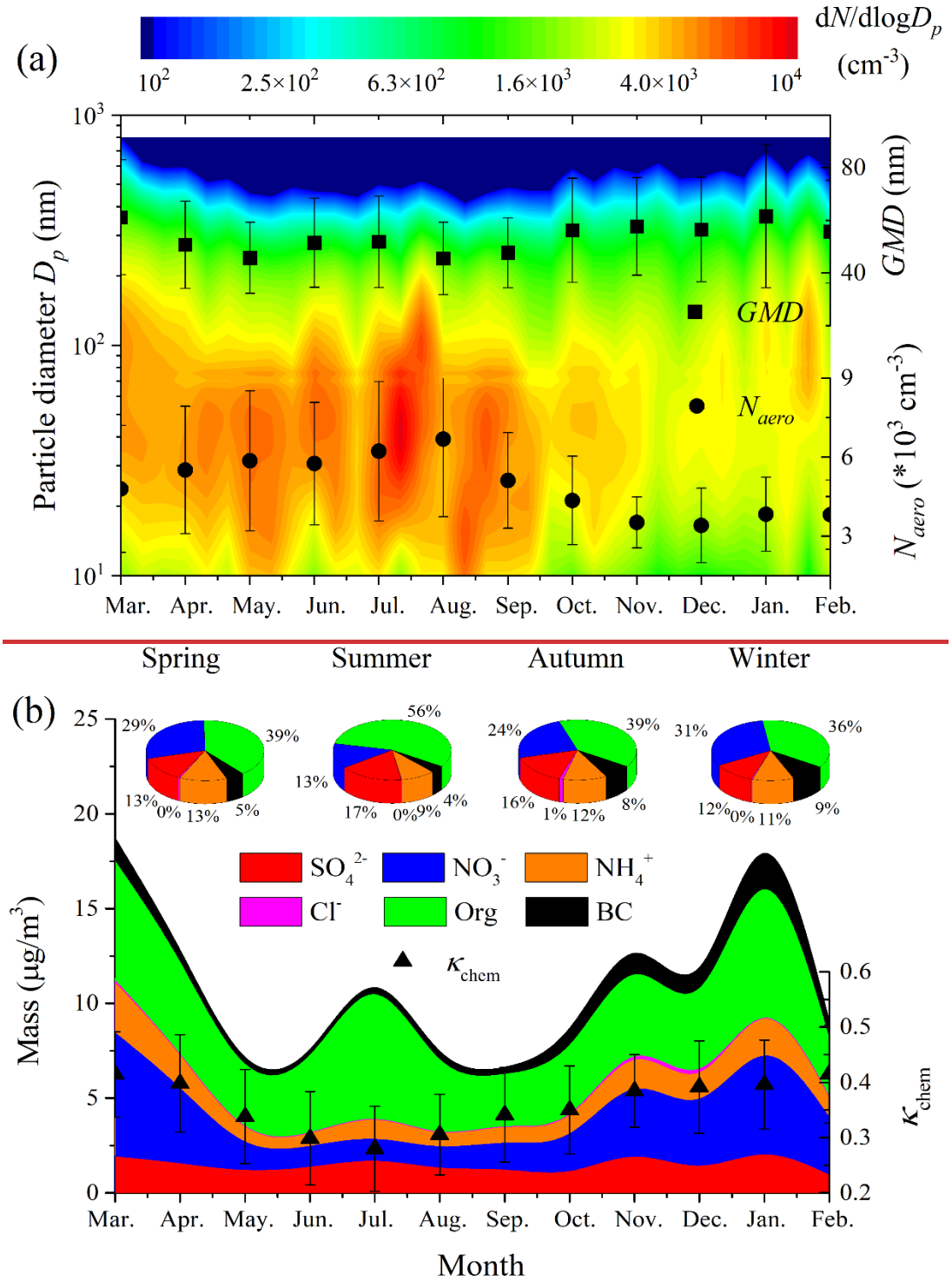
(a)
dN/dlogDp
(cm-3)
10^2
2.5×10^2
6.3×10^2
1.6×10^3
4.0×10^3
10^4
Particle diameter Dp (nm)
GMD (nm)
Naero (*10^3 cm-3)
GMD
Naero
Mar. Apr. May. Jun. Jul. Aug. Sep. Oct. Nov. Dec. Jan. Feb.
Spring
Summer
Autumn
Winter
(b)
Mass (μg/m3)
SO4 2-
NO3 -
NH4 +
Cl-
Org
BC
κchem
Month

1296

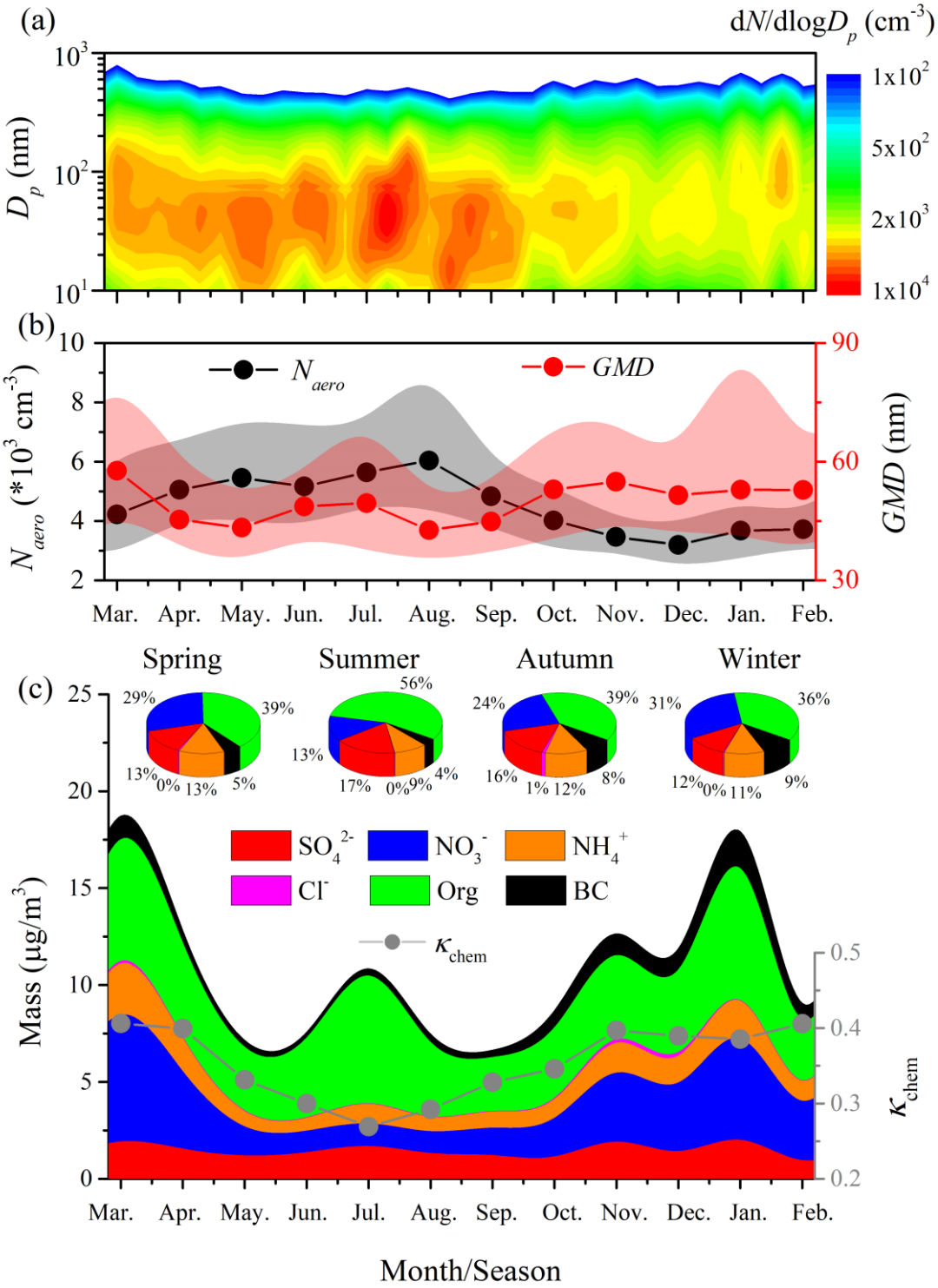

Figure 4. Seasonal variations of (a) aerosol particle number size distribution ($dN_{aero}/dlogD_p$ vs. D_p, D_p is particle diameter), (b) total aerosol number concentration with a D_p range of 10 to 800 nm (N_{aero}) and geometric mean diameter of the particles (*GMD*), and (c) mass concentration and ratio of each component in aerosol particle with D_p less than 1 μm and the hygroscopicity factor calculated from the chemical composition (κ_{chem}). Dots represent the median values. Shaded areas

represent the values in the range from 25th to 75th percent.~~Seasonal variations of (a) aerosol physical and (b) chemical properties. dN_{aero}/dlog$D$ represents the aerosol number concentration at each bin, GMD is the geometric mean diameter of the particles, N_{aero} means total aerosol number concentration with diameter ranging 10 to 800 nm, κ_{chem} is the hygroscopicity factor calculated from the chemical composition. Error bar is one standard derivation.~~

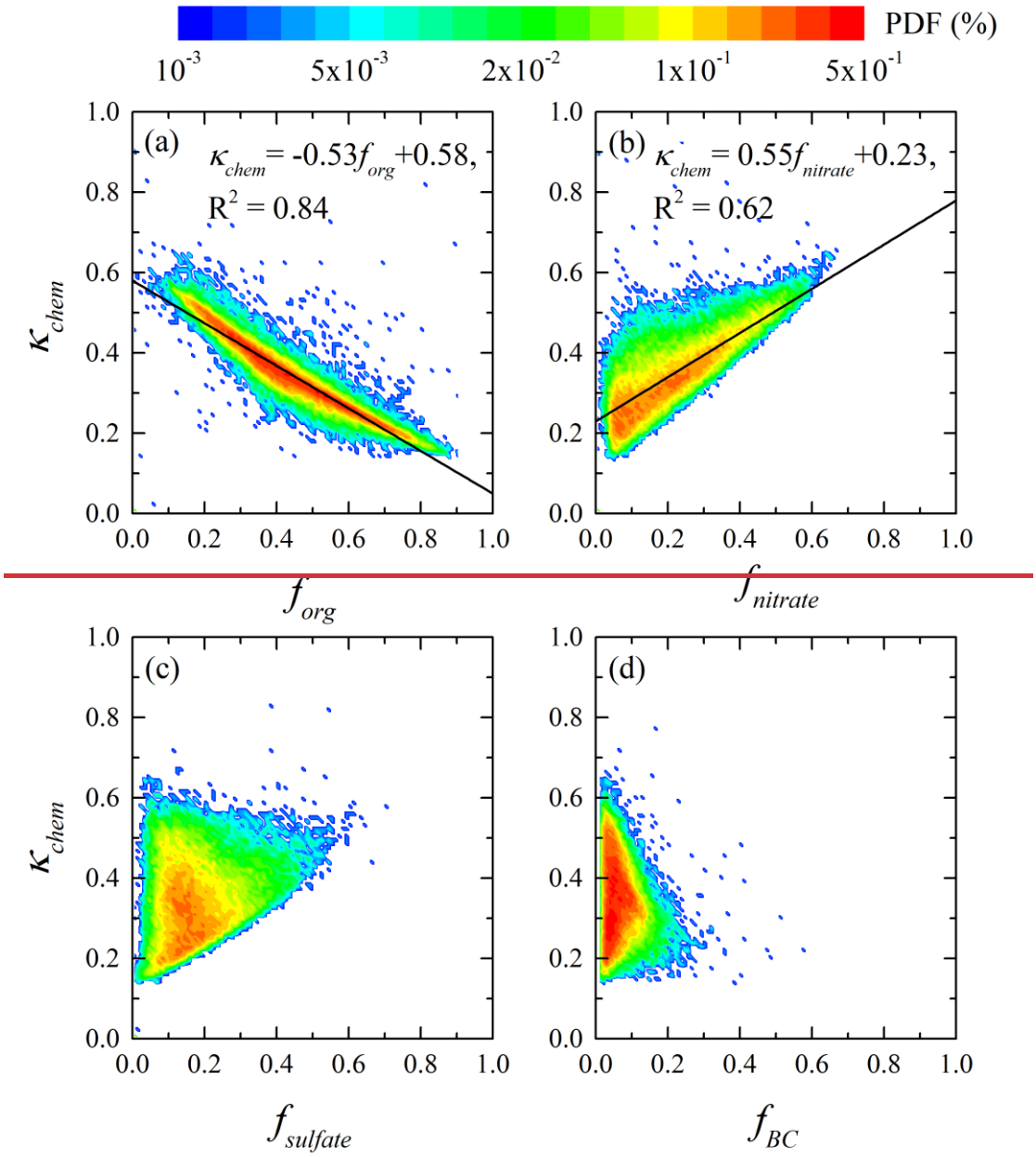

~~Figure 5. Relationships between (a) aerosol hygroscopicity factor calculated from the chemical composition (κ_{chem}) and mass fraction of organics (f_{org}) in submicron aerosol, (b) κ_{chem} vs. mass fraction of nitrate ($f_{nitrate}$), (c) κ_{chem} vs. mass fraction of nitrate ($f_{sulfate}$), and (d) κ_{chem} vs. mass fraction~~

~~of black carbon (f_{BC}). Color bar represents the probability density function (PDF). Black lines are linear fit lines.~~

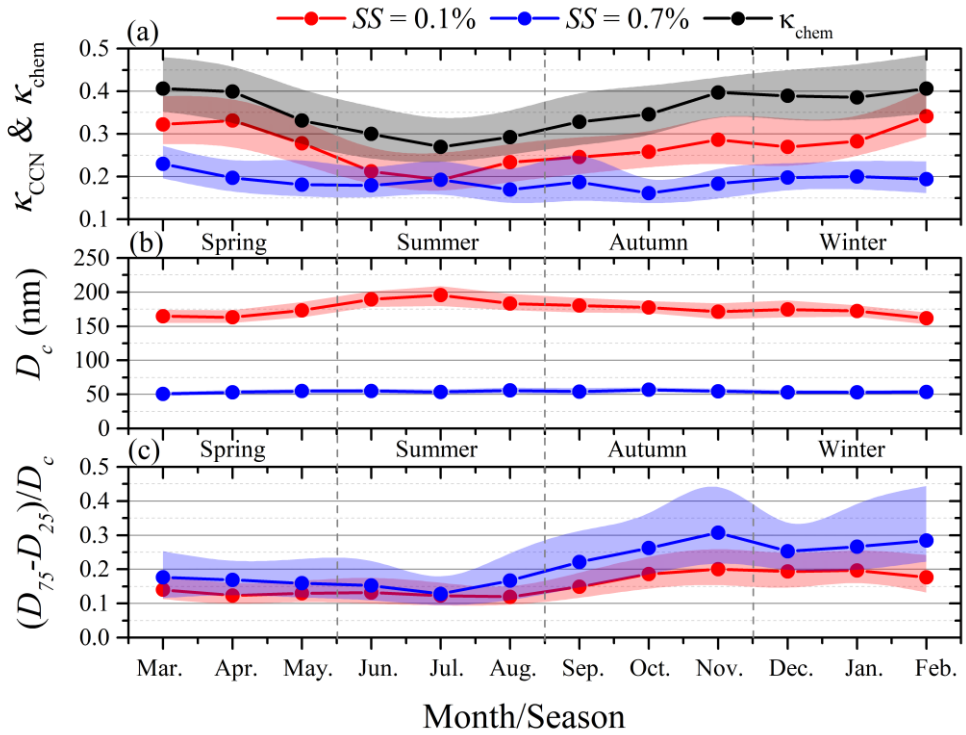

Figure 5. Monthly variations of (a) hygroscopicity factor calculated from monodisperse CCN measurements (κ_{CCN}) at supersaturation (SS) of 0.1% and 0.7%, and hygroscopicity factor calculated from particle chemical composition (κ_{chem}), (b) critical diameter of dry particle for activation (D_c) at SS = 0.1% and 0.7%, and (c) the degree of external mixture ((D_{75} – D_{25})/D_c) at SS = 0.1% and 0.7%. The definitions of D_{75} and D_{25} are the D_p at which 75% and 25% of the particles are activated at the given SS, respectively. Dots represent the median values. Shaded areas represent the values in the range from 25th to 75th percent.

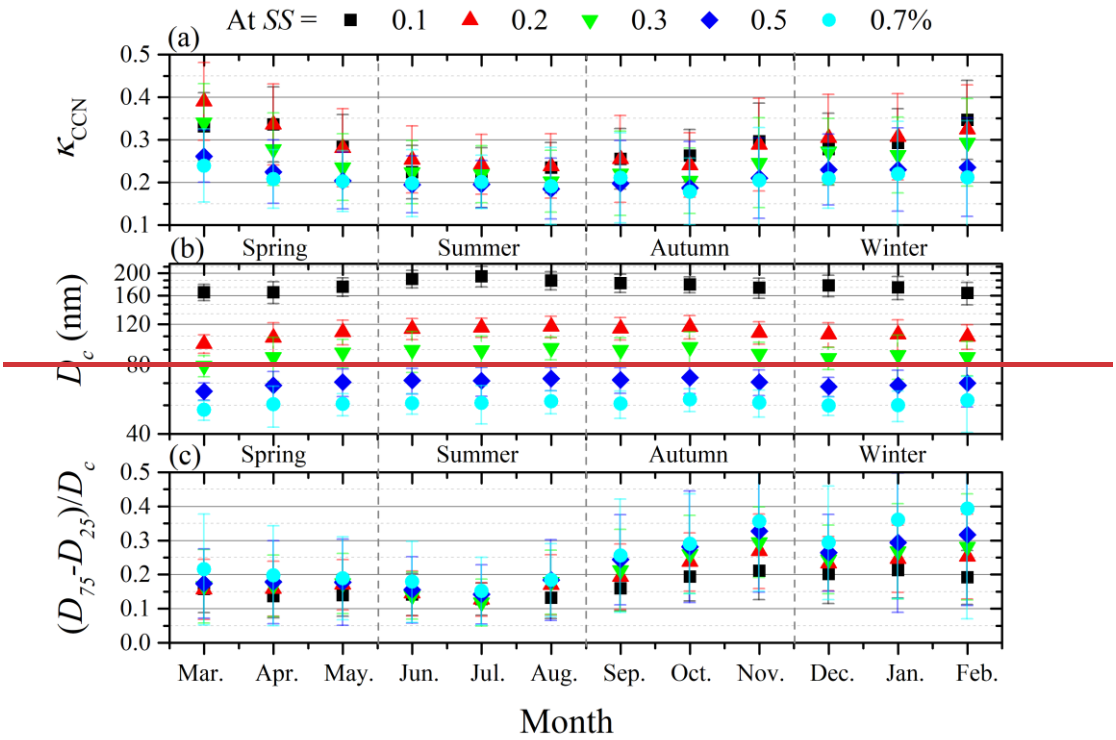

~~Figure 6. Monthly average of (a) hygroscopicity factor calculated from monodisperse CCN measurements (κ_{CCN}), (b) critical diameter of dry particle for activation (D_c), and (c) the degree of external mixture ($(D_{75}-D_{25})/D_c$) at five different supersaturation (SS) conditions. The definitions of D_{75} and D_{25} are the D_p at which 75% and 25% of the particles are activated at the given SS, respectively. Error bar is one standard derivation.~~

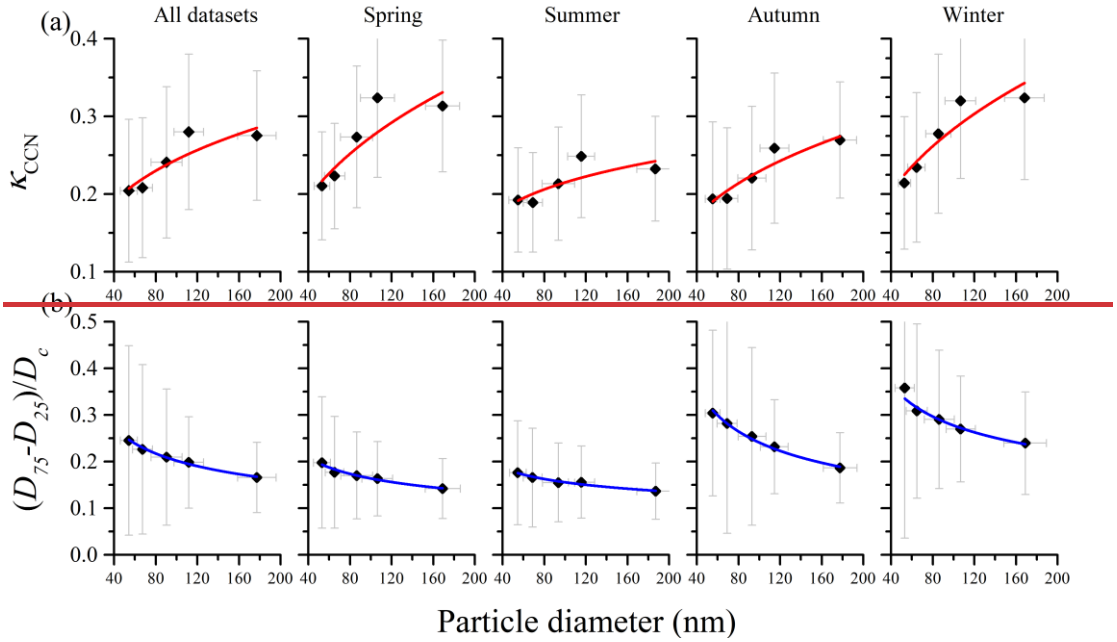

~~Figure 7. (a) Relationship between the particle diameter (D_p) and hygroscopicity factor calculated from monodisperse CCN measurements (κ_{CCN}), and (b) D_p vs. degree of external mixture ((D_{75}–D_{25})/D_c) at each season. The definitions of D_{75} and D_{25} are the D_p at which 75% and 25% of the particles are activated at the given *SS*, respectively. Red and blue lines are power-law fits for κ_{CCN} vs. D_p and (D_{75} – D_{25})/D_c vs. D_p.~~

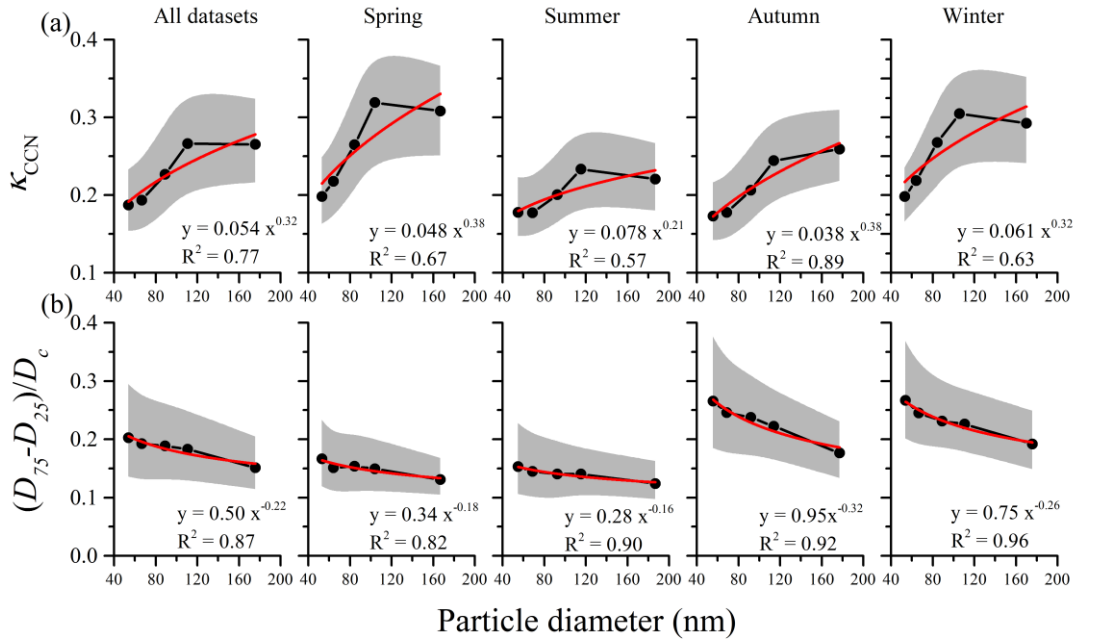

Figure 6. (a) Relationship between the hygroscopicity factor calculated from monodisperse CCN measurements (κ_{CCN}) and particle diameter (D_p), and (b) degree of external mixture ((D_{75} – D_{25})/D_c)

vs. D_p at each season. The definitions of D_{75} and D_{25} are the D_p at which 75% and 25% of the particles are activated at the given *SS*, respectively. Red lines are power-law fits. Dots represent the median values. Shaded areas represent the values in the range from 25th to 75th percent.

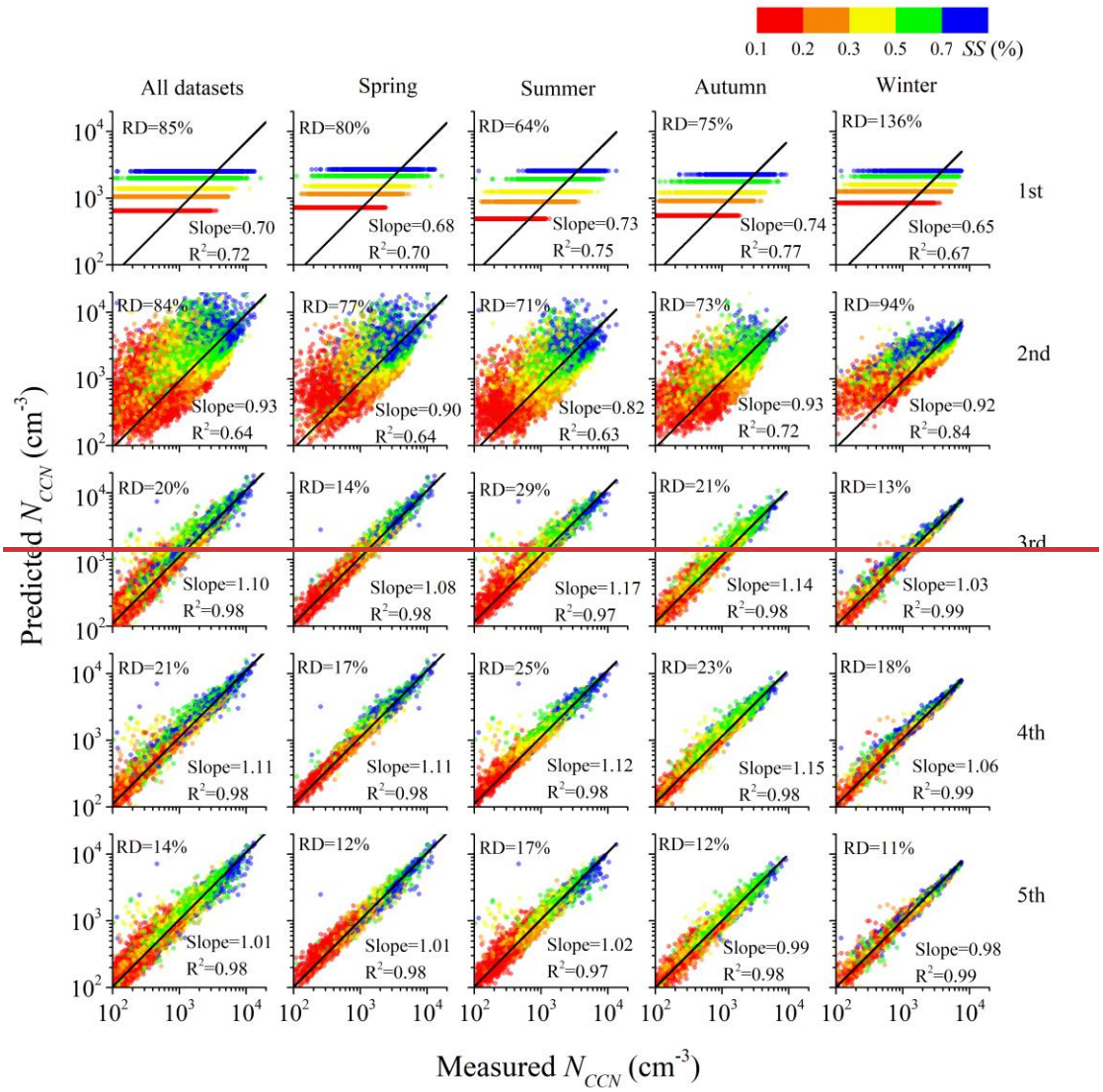

~~Figure 8. Predicted vs. measured CCN number concentration (N_{CCN}) for different seasons. The Predicted N_{CCN} is calculated from five different schemes with a detailed introduction shown in Table 6. Color bar represents the different supersaturation (*SS*) conditions. Black lines are the linear fits. The slope and R^2 of the linear regression and the relative deviation (RD) of the predicted N_{CCN} (RD= (|predicted N_{CCN} – measured N_{CCN}|)/measured N_{CCN}) are shown in each panel. Each row represents the results at the same scheme in different seasons; each column represents the results at different schemes in the same season.~~

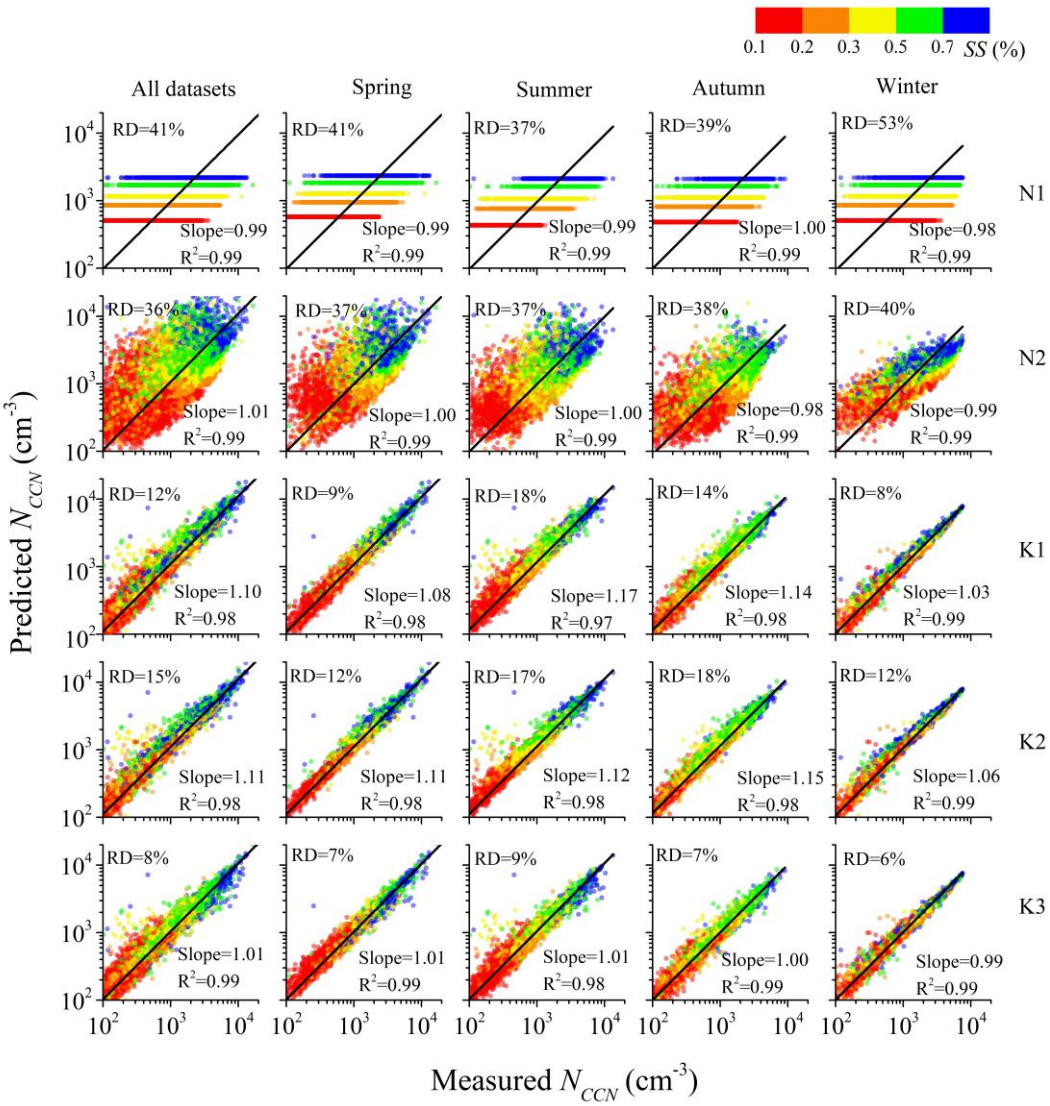

Figure 7. Predicted vs. measured CCN number concentration (N_{CCN}) for different seasons. The Predicted N_{CCN} is calculated from five different schemes with a detailed introduction shown in Table 3. Color bar represents the different supersaturation (*SS*) conditions. Black lines are the linear fits. The slope and R^2 of the linear regression and the median relative deviation (RD) between the predicted and measured N_{CCN} are shown in each panel. Each row represents the results using the same scheme in different seasons. Each column represents the results using different schemes in the same season.

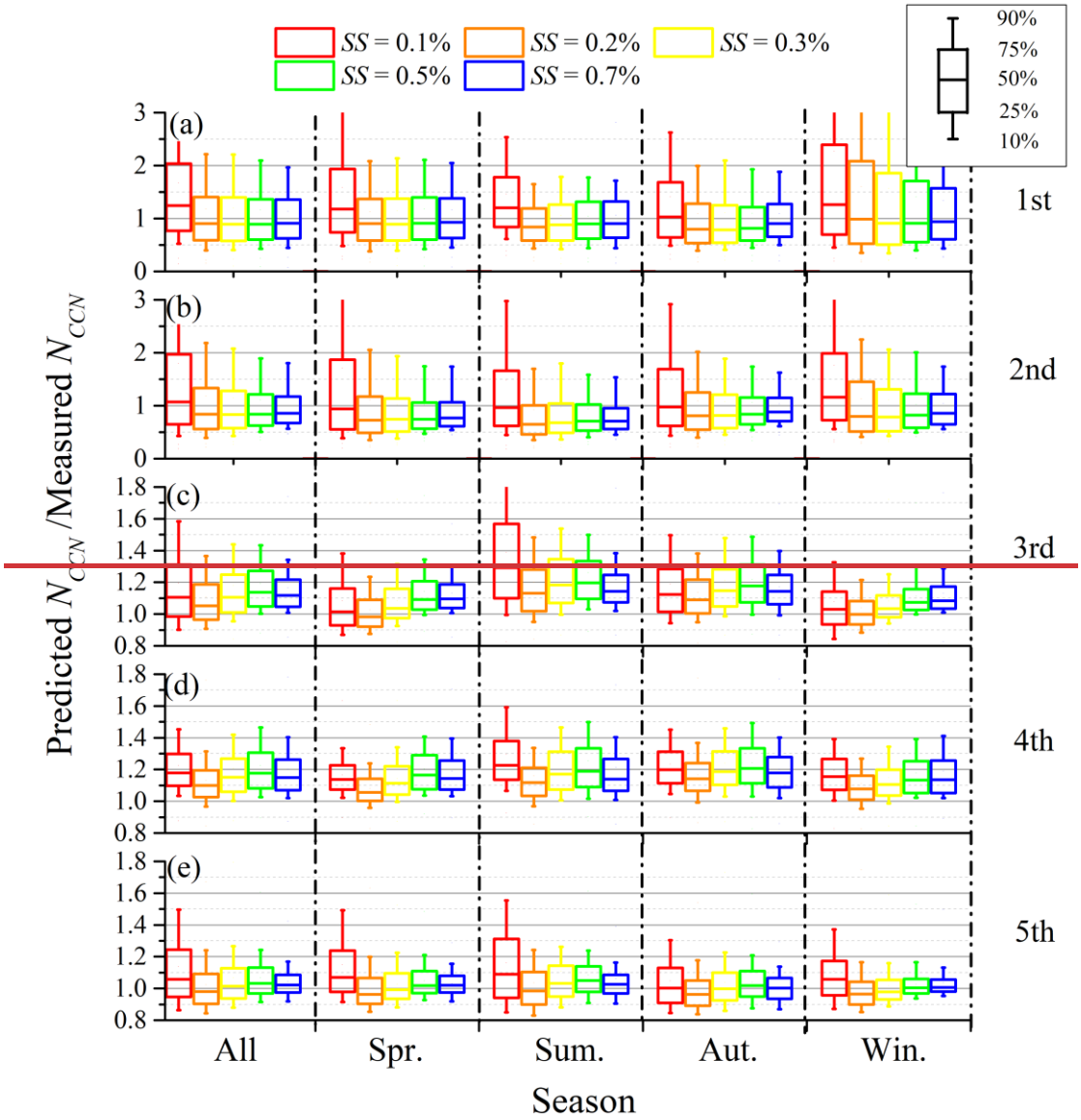

~~Figure 9. Statistics of the ratio of predicted CCN number concentration (N_{CCN}) to the measured one at different supersaturation (*SS*) conditions for each season and all datasets. The (a), (b), (c), (d), and (e) represent the prediction results from the 1st, 2nd, 3rd, 4th, and 5th scheme, respectively.~~

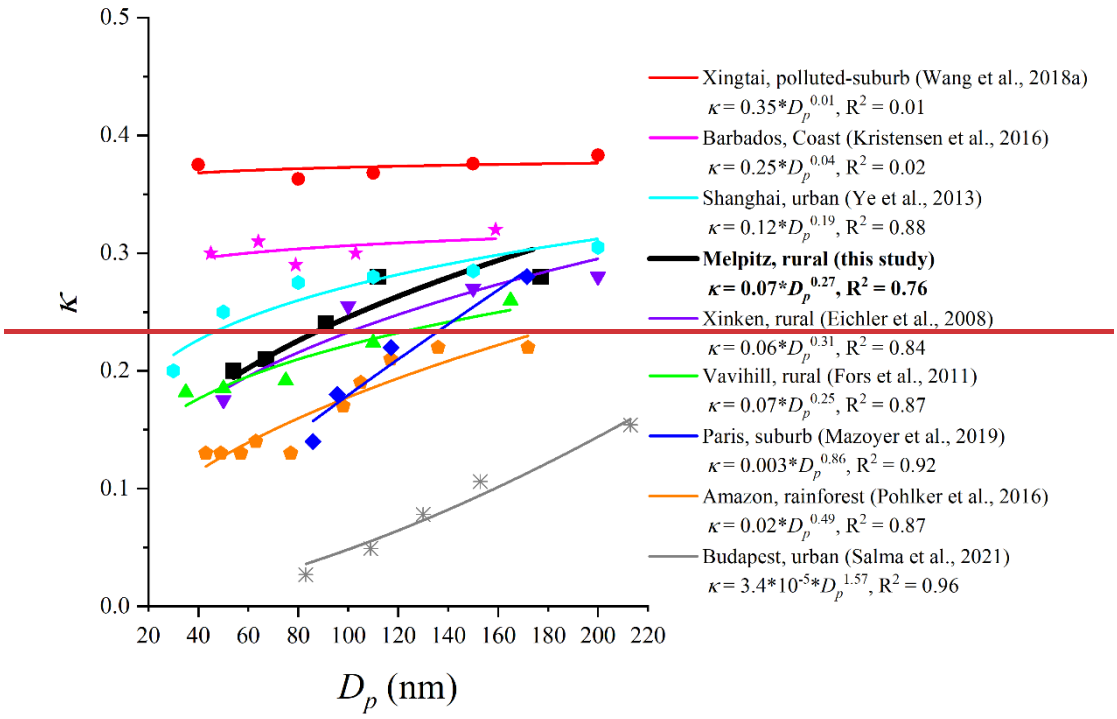

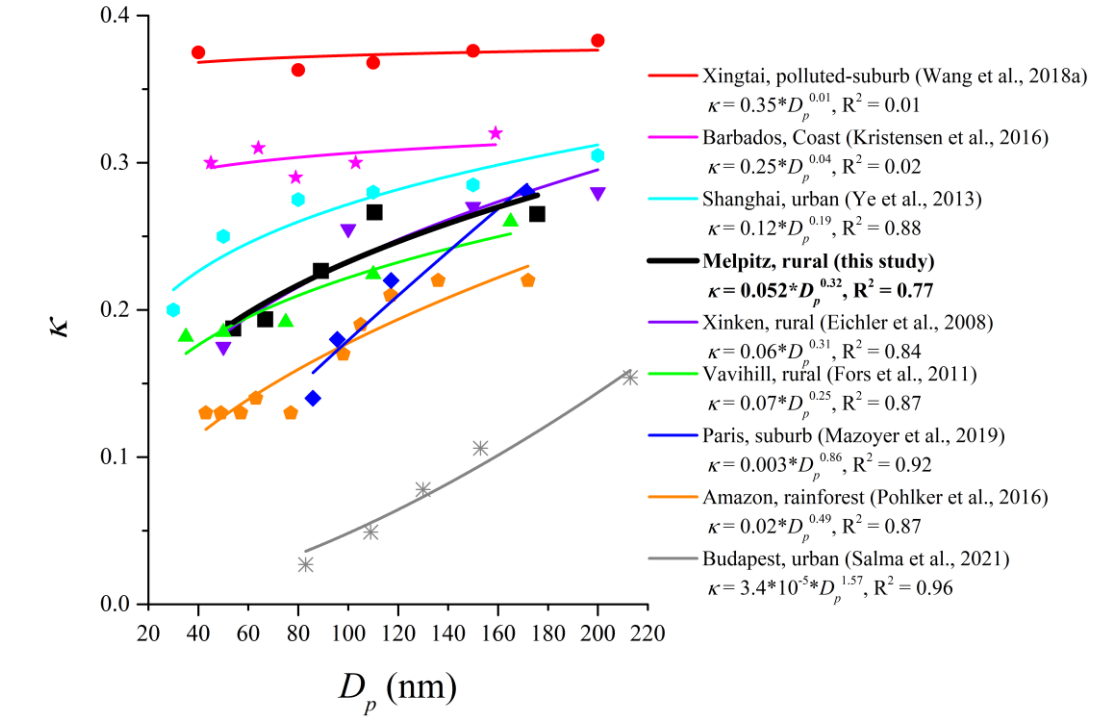

Figure 8~~10~~. Relationships between the particle hygroscopicity factor (κ) and diameter (D_p) observed at different aerosol background regions. Lines are ~~the~~ power-law fits of κ vs. D_p.

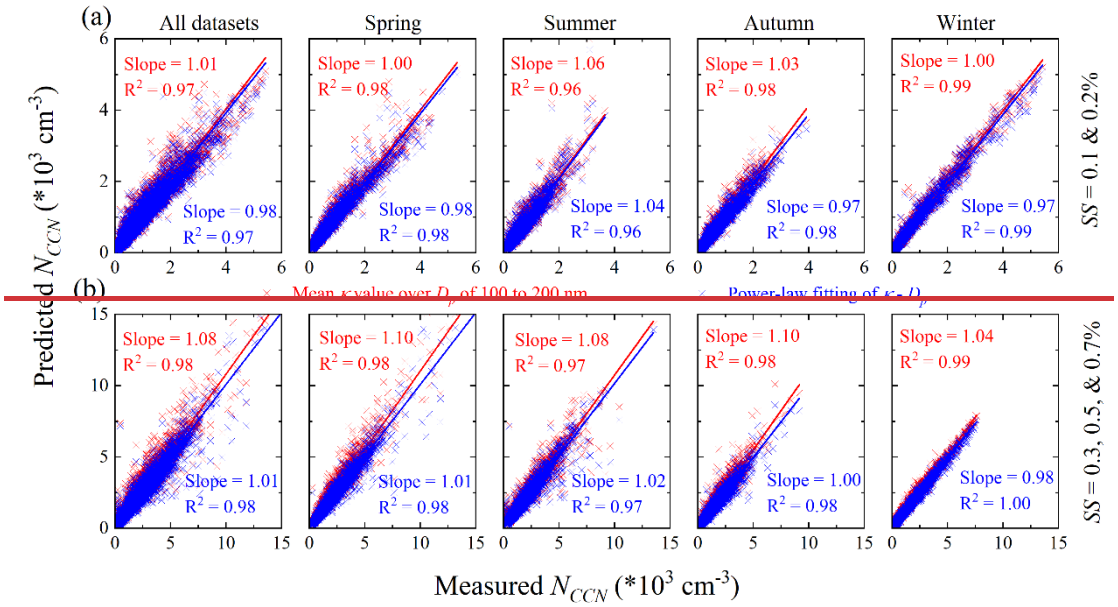

~~Figure 11. Predicted vs. measured CCN number concentration (N_{CCN}) at different supersaturation (SS) conditions for different seasons. (a) represents the results at SS = 0.1 and 0.2%; (b) shows the results at SS = 0.3, 0.5, and 0.7%. Red cross represents the predicted N_{CCN} using mean hygroscopicity factor (κ) over particle diameter (D_p) of 100 to 200 nm, while the blue cross represents the predicted N_{CCN} using power-law fit of κ and D_p. Red and blue lines are the linear fits.~~

Table 1. Densities (ρ) and hygroscopicity factor (κ) for each component.

Species	NH_4NO_3	$(NH_4)_2SO_4$	NH_4HSO_4	H_2SO_4	Organics	BC
ρ (kg m^{-3})	1720	1769	1780	1830	1400	1700
κ	0.67	0.61	0.61	0.92	0.1	0

~~Table 2. Summary of CCN number concentration (N_{CCN}) at different supersaturation (SS) conditions measured at different locations.~~

~~Location (coordinates; a.m.s.l)~~	~~Type~~	~~Period~~	~~SS (%)~~	~~Mean N_{CCN} (cm^{-3})~~	~~Reference~~
~~Melpitz, Germany (51.5°N, 12.9°E; 86 m)~~	~~rural, continental~~	~~Aug. 2012–Oct. 2016~~	~~0.1~~ ~~0.2~~ ~~0.3~~ ~~0.5~~ ~~0.7~~	~~513~~ ~~1102~~ ~~1466~~ ~~2020~~ ~~2477~~	~~Present study~~
~~Vavihill, Sweden (56.0°N, 13.2 °E; 172 m)~~	~~rural~~	~~May 2008–Jul 2010~~	~~0.1–1.0~~	~~362–1795~~	~~Fors et al., 2011~~
~~Southern Great Plains, USA (36.6°N, 97.5°W; 320 m)~~	~~rural, agricultural~~	~~Sep. 2006–Apr. 2011~~	~~0.4~~	~~1248~~	~~Liu and Li, 2014~~
~~Hyytiälä, Finland (61.9°N, 24.3°E; 181 m)~~	~~rural~~	~~Feb. 2009–Dec. 2012~~	~~0.1–1.0~~	~~274–1128~~	~~Paramonov et al., 2015~~
~~Mahabaleshwar, India (17.9°N, 73.7°E; ~490 m)~~	~~rural~~	~~Jun. 2015~~	~~0.1–0.94~~	~~118–1826~~	~~Singla et al., 2017~~
~~Guangzhou, China (23.6°N, 113.1°E; ~21 m)~~	~~rural~~	~~Jul. 2006~~	~~0.068–0.67~~	~~995–10731~~	~~Rose et al., 2010~~
~~Wuqing, China (39.4°N, 117.0°E; 7.4 m)~~	~~suburban~~	~~Dec. 2009–Jan. 2010~~	~~0.056–0.7~~	~~2192–12963~~	~~Deng et al., 2011~~
~~Seoul, Korea (37.6°N, 127.0°E; ~38 m)~~	~~urban~~	~~2004–2010~~	~~0.4–0.8~~	~~4145–6067~~	~~Kim et al., 2014~~
~~Mahabubnagar, India (17.7°N, 78.9°E; ~490 m)~~	~~polluted continental~~	~~Oct. 2011~~	~~1.0~~	~~~5400~~	~~Varghese et al., 2016~~

~~Table 3. Power-law function fits and error function fits for the relationships between activation ratio (AR) vs. supersaturation (*SS*), and CCN number concentration (N_{CCN}) vs. *SS* for different seasons.~~

~~Season~~	~~*AR* vs. *SS*~~		~~N_{CCN} vs. *SS*~~	
	~~*Power-law*~~	~~*Error Function*~~	~~*Power-law*~~	~~*Error Function*~~
~~Spring~~	~~$AR=0.66SS^{0.73}$, $R^2=0.98$~~	~~$AR=0.5+0.50\mathrm{erf}(\ln(SS/0.72)/2.33)$, $R^2=0.998$~~	~~$N_{CCN}=3679SS^{0.76}$, $R^2=0.97$~~	~~$N_{CCN}=2637+2637\mathrm{erf}(\ln(SS/0.72)/2.33)$, $R^2=0.998$~~
~~Summer~~	~~$AR=0.61SS^{0.97}$, $R^2=0.97$~~	~~$AR=0.51+0.51\mathrm{erf}(\ln(SS/1.04)/2.15)$, $R^2=0.997$~~	~~$N_{CCN}=3951SS^{1.01}$, $R^2=0.96$~~	~~$N_{CCN}=3162+3162\mathrm{erf}(\ln(SS/1.04)/2.15)$, $R^2=0.997$~~
~~Autumn~~	~~$AR=0.71SS^{0.79}$, $R^2=0.98$~~	~~$AR=0.56+0.56\mathrm{erf}(\ln(SS/0.84)/2.29)$, $R^2=0.999$~~	~~$N_{CCN}=3136SS^{0.81}$, $R^2=0.98$~~	~~$N_{CCN}=2433+24336\mathrm{erf}(\ln(SS/0.84)/2.29)$, $R^2=0.999$~~
~~Winter~~	~~$AR=0.89SS^{0.63}$, $R^2=0.96$~~	~~$AR=0.44+0.44\mathrm{erf}(\ln(SS/0.29)/1.83)$, $R^2=0.999$~~	~~$N_{CCN}=3325SS^{0.64}$, $R^2=0.96$~~	~~$N_{CCN}=1624+1624\mathrm{erf}(\ln(SS/0.29)/1.83)$, $R^2=0.999$~~
~~All~~	~~$AR=0.59SS^{0.71}$, $R^2=0.98$~~	~~$AR=0.40+0.40\mathrm{erf}(\ln(SS/0.59)/2.25)$, $R^2=0.998$~~	~~$N_{CCN}=3497SS^{0.81}$, $R^2=0.98$~~	~~$N_{CCN}=2199+2199\mathrm{erf}(\ln(SS/0.59)/2.25)$, $R^2=0.998$~~

~~Table 4. At each supersaturation (*SS*) condition, seasonal mean values of the hygroscopicity factor calculated from monodisperse CCN measurements (κ_{CCN}), the critical diameter of dry particle for activation (D_e), and the degree of external mixture (($D_{75}-D_{25}$)/D_e). The unit of D_e is nm.~~

~~Parameters~~	~~*SS* (%)~~	~~All datasets~~	~~Spring~~	~~Summer~~	~~Autumn~~	~~Winter~~
~~κ_{CCN}~~	~~0.1~~	~~0.28~~	~~0.31~~	~~0.23~~	~~0.27~~	~~0.32~~
	~~0.2~~	~~0.28~~	~~0.32~~	~~0.25~~	~~0.26~~	~~0.32~~
	~~0.3~~	~~0.24~~	~~0.27~~	~~0.21~~	~~0.22~~	~~0.28~~
	~~0.5~~	~~0.21~~	~~0.22~~	~~0.19~~	~~0.19~~	~~0.23~~
	~~0.7~~	~~0.20~~	~~0.21~~	~~0.19~~	~~0.19~~	~~0.21~~
~~D_e~~	~~0.1~~	~~177~~	~~169~~	~~187~~	~~178~~	~~168~~
	~~0.2~~	~~112~~	~~107~~	~~116~~	~~115~~	~~107~~
	~~0.3~~	~~91~~	~~87~~	~~94~~	~~93~~	~~86~~
	~~0.5~~	~~67~~	~~65~~	~~69~~	~~69~~	~~64~~
	~~0.7~~	~~54~~	~~53~~	~~55~~	~~55~~	~~53~~
~~($D_{75}-D_{25}$)/D_e~~	~~0.1~~	~~0.17~~	~~0.14~~	~~0.14~~	~~0.19~~	~~0.24~~
	~~0.2~~	~~0.20~~	~~0.16~~	~~0.16~~	~~0.23~~	~~0.27~~
	~~0.3~~	~~0.21~~	~~0.17~~	~~0.15~~	~~0.25~~	~~0.29~~
	~~0.5~~	~~0.23~~	~~0.18~~	~~0.17~~	~~0.28~~	~~0.31~~
	~~0.7~~	~~0.25~~	~~0.20~~	~~0.18~~	~~0.30~~	~~0.36~~

Table2. Seasonal median values of hygroscopicity factor derived from the chemical composition (κ_{chem}), hygroscopicity factor derived from monodisperse CCN measurements (κ_{CCN}), the critical diameter of dry particle for activation (D_c), and the degree of external mixture (($D_{75} - D_{25}$)/D_c) at each supersaturation (SS) condition. The unit of D_c is nm.

Parameters	SS (%)	All datasets	Spring	Summer	Autumn	Winter
κ_{chem}	-	0.30	0.32	0.24	0.31	0.34
κ_{CCN}	0.1	0.27	0.31	0.22	0.26	0.29
	0.2	0.27	0.32	0.23	0.24	0.30
	0.3	0.23	0.26	0.20	0.21	0.27
	0.5	0.19	0.22	0.18	0.18	0.22
	0.7	0.19	0.20	0.18	0.17	0.20
D_c	0.1	176	167	187	177	170
	0.2	111	104	116	114	106
	0.3	89	85	93	92	84
	0.5	67	64	69	69	64
	0.7	54	53	55	55	53
($D_{75} - D_{25}$) /D_c	0.1	0.15	0.13	0.12	0.18	0.19
	0.2	0.18	0.15	0.14	0.22	0.23
	0.3	0.19	0.15	0.14	0.24	0.23
	0.5	0.20	0.15	0.14	0.25	0.25
	0.7	0.20	0.17	0.15	0.27	0.27

~~Table 5. Power-law fit results in Figure 7. The unit of particle diameter (D_p) is nm.~~

	~~κ_{CCN} vs. D_p~~	~~$(D_{75}-D_{25})/D_c$ vs. D_p~~
~~All datasets~~	~~$y = 0.07\ x^{0.27}$, $R^2 = 0.76$~~	~~$y = 0.92\ x^{-0.33}$, $R^2 = 0.99$~~
~~Spring~~	~~$y = 0.05\ x^{0.37}$, $R^2 = 0.76$~~	~~$y = 0.55\ x^{-0.26}$, $R^2 = 0.97$~~
~~Summer~~	~~$y = 0.09\ x^{0.19}$, $R^2 = 0.56$~~	~~$y = 0.39\ x^{-0.20}$, $R^2 = 0.95$~~
~~Autumn~~	~~$y = 0.05\ x^{0.31}$, $R^2 = 0.88$~~	~~$y = 1.70\ x^{-0.42}$, $R^2 = 0.99$~~
~~Winter~~	~~$y = 0.05\ x^{0.36}$, $R^2 = 0.82$~~	~~$y = 1.10\ x^{-0.30}$, $R^2 = 0.95$~~

Table ~~6~~3. Introduction of five activation schemes. The meaning of the abbreviation can be found in Notation list.

Category	Scheme	Introduction
1st category: N_{CCN} - SS or AR - SS empirical fit	N1~~1st~~	N_{CCN} - SS power-law fits shown in ~~Table 3~~Figure 3a
	N2~~2nd~~	Real-time N_{aero} combined with AR - SS power-law fits shown in Figure 3a~~Table 3~~
2nd category: Real-time PNSD combined with the parameterized κ	K1~~3rd~~	Real-time PNSD combined with a constant κ of 0.3
	K2~~4th~~	Real-time PNSD combined with the real-time bulk κ_{chem}
	K3~~5th~~	Real-time PNSD combined with κ - D_p power-law fits shown in ~~Table 5~~Figure 6a

~~**Appendix A**~~

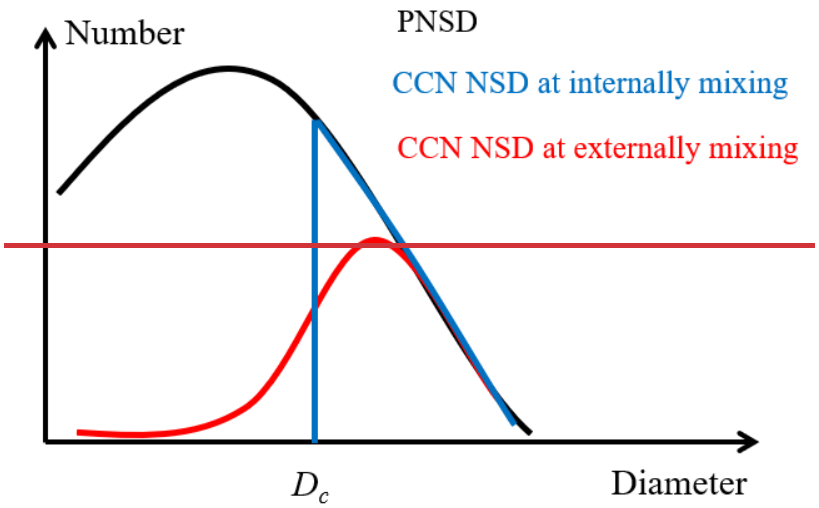

~~Figure A1. Schematic diagram for the relationship among the particle number size distribution (PNSD), CCN number size distribution (CCN NSD) at internally mixing, and the CCN NSD at externally mixing.~~